Sheffield Hallam University

Label-free Quantitative Proteomics and Substrate Based Mass Spectrometry Imaging of Xenobiotic Metabolizing Enzymes in ex Vivo Human Skin and a Human Living Skin Equivalent Model.

COUTO, Narciso <http://orcid.org/0000-0001-7565-4357>, NEWTON, Jillian R.A., RUSSO, Cristina, KARUNAKARAN, Esther, ACHOUR, Brahim <http://orcid.org/0000-0002-2595-5626>, AL-MAJDOUB, Zubida M. <http://orcid.org/0000-0002-1497-3140>, SIDAWAY, James, ROSTAMI-HODJEGAN, Amin, CLENCH, Malcolm R. <http://orcid.org/0000-0002-0798-831X> and BARBER, Jill <http://orcid.org/0000-0002-5424-0291>

Available from Sheffield Hallam University Research Archive (SHURA) at:

https://shura.shu.ac.uk/27828/

This document is the Accepted Version [AM]

Citation:

COUTO, Narciso, NEWTON, Jillian R.A., RUSSO, Cristina, KARUNAKARAN, Esther, ACHOUR, Brahim, AL-MAJDOUB, Zubida M., SIDAWAY, James, ROSTAMI-HODJEGAN, Amin, CLENCH, Malcolm R. and BARBER, Jill (2021). Label-free Quantitative Proteomics and Substrate Based Mass Spectrometry Imaging of Xenobiotic Metabolizing Enzymes in ex Vivo Human Skin and a Human Living Skin Equivalent Model. Drug Metabolism and Disposition. [Article]

Copyright and re-use policy

See http://shura.shu.ac.uk/information.html

Sheffield Hallam University Research Archive
http://shura.shu.ac.uk

Label-free Quantitative Proteomics and Substrate Based Mass Spectrometry Imaging of Xenobiotic Metabolizing Enzymes in ex Vivo Human Skin and a Human Living Skin Equivalent Model

Narciso Couto[1,2,4], Jillian R. A. Newton[3], Cristina Russo[3], Esther Karunakaran[1,4], Brahim Achour[2], Zubida M. Al-Majdoub[2], James Sidaway[5], Amin Rostami-Hodjegan[2,6], Malcolm R. Clench[3], Jill Barber[2]*

[1] Department of Chemical and Biological Engineering, University of Sheffield, Sir Robert Hadfield Building, Mappin Street, Sheffield S1 3JD, UK.

[2] Centre for Applied Pharmacokinetic Research, University of Manchester, Stopford Building, Oxford Road, Manchester, M13 9PT, UK.

[3] Centre for Mass Spectrometry Imaging, Biomolecular Sciences Research Centre, Sheffield Hallam University, Howard Street, Sheffield, S1 1WB, UK.

[4] Sheffield Collaboratorium for Antimicrobial Resistance and Biofilms (SCARAB), University of Sheffield, Sheffield, S1 3JD, UK.

[5] Phenotox Ltd, Bollington, UK

[6] Simcyp Ltd. (a Certara company), 1 Concourse Way, Sheffield, S1 2BJ, UK.

Running title: Quantification of xenobiotic-metabolizing enzymes in human skin and an equivalent model.

Correspondent authors:

n.couto@sheffield.ac.uk, ORCID ID: 0000-0001-7565-4357

jill.barber@manchester.ac.uk, ORCID: 0000-0002-5424-0291

Number of Pages: 43

Number of Tables: 6

Number of Figures: 5

Number of References: 41

Words in Abstract: 221

Words in Introduction: 673

Words in Discussion: 1970

Abbreviations

CYP, cytochrome P450; UGT, uridine 5'-diphosphate-glucuronosyltransferase; ABC, ATP-binding cassette; SLC, solute carrier; FASP, filter-aided sample preparation; LC-MS/MS, liquid chromatography-tandem mass spectrometry; SBMSI, substrate based mass spectrometry imaging.

Abstract

We report for the first time label-free quantification of xenobiotic metabolizing enzymes (XME), transporters, redox enzymes, proteases and nucleases in six human skin explants and a 3D living skin equivalent model from LabSkin. We aimed to evaluate the suitability of LabSkin as an alternative to animal testing for the development of topical formulations. More than 2000 proteins were identified and quantified from total cellular protein. Alcohol dehydrogenase 1C (ADH1C), the most abundant phase I XME in human skin, and glutathione S-transferase pi 1 (GSTP1), the most abundant phase II XME in human skin, were present in similar abundance in LabSkin. Several esterases were quantified and esterase activity was confirmed in LabSkin using substrate-based mass spectrometry imaging. No cytochrome P450 (CYP) activity was observed for the substrates tested, in agreement with the proteomics data, where the cognate CYPs were absent in both human skin and LabSkin. Label-free protein quantification allowed insights into other related processes such as redox homeostasis and proteolysis. For example, the most abundant antioxidant enzymes were thioredoxin (TXN) and peroxiredoxin-1 (PRDX1). This systematic determination of functional equivalence between human skin and LabSkin is a key step towards the construction of a representative human *in vitro* skin model, which can be used as an alternative to current animal-based tests for chemical safety and for predicting dosage of topically administered drugs.

Significance

The use of label-free quantitative mass spectrometry to elucidate the abundance of xenobiotic metabolizing enzymes, transporters, redox enzymes, proteases and nucleases in human skin enhance our understanding of the skin physiology and biotransformation of topical drugs and cosmetics. This will help develop mathematical models to predict drug metabolism in human skin and to develop more robust *in vitro* engineered human skin tissue as alternatives to animal testing.

Introduction

In Europe, testing cosmetic products on animals has been banned since 2009 because of the 7th amendment of the EU Cosmetics Directive. Animals are, however, still used for testing the majority of new topical drugs. Efforts have been made worldwide to replace, reduce, and refine animal use in drug development and to implement reliable non-animal alternative tests for predicting safety and/or toxicity of drugs and cosmetics. *In vitro* 3D laboratory models of human skin are candidate alternatives for the development of cosmetics as well as drugs. Several 3D skin models have been developed (Cantòn *et al.*, 2010; Chau *et al.*, 2013; Mathes *et al.*, 2014), but none has been satisfactorily validated against human skin, in part because we lack understanding of xenobiotic-metabolizing enzyme (XME) pathways in human skin. The relatively few published studies on drug metabolism in human skin have mainly focussed on identifying and quantifying enzymes and pathways known to have a role in drug metabolism in other organs such as the liver and the intestine (Couto *et al.*, 2019, 2020; El-Khateeb *et al.*, 2019). Skin is a challenging tissue to analyse using traditional proteomic techniques owing to the high lipid content, and the insolubility and extensive cross-linking of proteins. This can complicate the isolation and digestion of proteins for analysis using mass spectrometry techniques. Consequently, the roles of XME and drug transporters in the human skin remain to be elucidated. We therefore set out to measure the levels of phase I and II XMEs and phase III drug transporters in *in vitro* skin models and compare them to human skin.

During xenobiotic metabolism, phase I and phase II enzymes activate xenobiotics by adding or revealing polar groups. Phase I enzymes include cytochrome P450 (CYP) enzymes, aldehyde oxidases (AOs), aldehyde dehydrogenases (ALDHs), aldo-ketoreductases (AKRs), alcohol dehydrogenases (ADHs), esterases, flavin-containing monooxygenases (FMOs) and cyclooxygenases (COXs). Enzymes from phase II include glutathione S-transferases (GSTs), UDP-

glucuronosyltransferases (UGTs), sulfotransferases (SULTs), N-acetyltransferases (NATs) and methyltransferases (MTs). The activated xenobiotics are subsequently transported to the bloodstream by a variety of phase III transporters from the adenosine triphosphate (ATP) binding cassette (ABC) and solute carrier (SLC) families (Kazem *et al.*, 2019).

Although these enzymes and transporters are the main players in xenobiotic disposition, biotransformation and transportation of xenobiotics are complex and dynamic processes where other enzymes and proteins can also play a direct or indirect role. For example, phase I metabolism produces reactive oxygen species, which, without control, cause oxidative stress and impair protein function (Couto *et al.*, 2013, 2016). However, the mechanism of reactive oxygen species generation during xenobiotic metabolism, association of XME in diseases, and the role of antioxidants and antioxidant enzymes in determining the effectiveness of xenobiotic metabolism have not been fully established. Given the important role of the antioxidant system in mediating the pharmacodynamics of drugs, it is necessary to understand antioxidant response to xenobiotics, the role of reactive oxygen species in toxicity and the role of antioxidant enzymes in modulating xenobiotic metabolism. It is also important to understand the roles of proteases, peptidases and protease inhibitors in skin because both cosmetics and emerging topical drug therapies increasingly incorporate bioactive peptides. In the human skin, the activity of peptidases and their inhibitors is tightly regulated. A breakdown in these regulatory mechanisms has been associated with a broad range of conditions such as cancer (Hu *et al.*, 2007) and inflammation (Overall and Dean, 2006).

Mass spectrometry-based quantitative proteomics is considered an excellent strategy to investigate metabolism in biological systems by quantifying protein abundance (Parker *et al.*, 2014; Russo *et al.*, 2016; Flores *et al.*, 2019; Raut *et al.*, 2019). To evaluate the potential for using *in vitro* laboratory models of human skin as viable alternatives to animal testing, a mass spectrometry-based approach

using both label-free quantitative proteomics and matrix-assisted laser desorption ionization (MALDI) imaging (Russo *et al.*, 2018) was undertaken in this study. The abundance of enzymes involved in xenobiotic metabolism including antioxidant enzymes, proteases, peptidases and nucleases were determined in an *in vitro* 3D human skin model (hereafter referred to as LabSkin) and compared with 6 human skin sections.

Materials and Methods

Chemicals

Unless, otherwise indicated, all chemicals were supplied by Sigma-Aldrich (Poole, Dorset, UK) with the highest purity available. Sequencing grade modified trypsin was supplied by Promega (Southampton, UK). All solvents were HPLC grade and supplied by ThermoFisher Scientific (Paisley, UK).

Human skin samples

Human skin tissues from one male and five female donors, were taken from “healthy” individuals undergoing routine abdominoplasty surgery. These human skin tissues were sourced by the Teaching Hospital from The University of Bradford. Ethics were approved for this study (36-DRMBPY-06-001) by the Independent Ethics Committee. All participants provided written informed consent and sample collection was conducted according to the principles expressed in the Declaration of Helsinki protocols.

3D LabSkin samples

LabSkin was supplied by LabSkin UK Ltd (York, UK). LabSkin was delivered after 14 days of development in transport culture medium. At the time of delivery, LabSkin was transferred into new deep 12 well plates, suspended in fresh LabSkin maintenance medium and left to incubate for 24h at 37°C with 5% CO_2, to normalise the metabolism.

Label-free quantification of proteins

Sample preparation

All procedures were performed with sterile equipment and solvents using aseptic techniques. Approximately 3 g of human skin tissue and 1.5 g of LabSkin were washed twice with 10 mL of washing buffer (250 mM phosphate buffer pH 7.4, 150 mM potassium chloride, 1 mM EDTA). From the human tissues, the subcutaneous layer was removed before skin samples were cut into small pieces with sterile forceps and surgical scalpels. LabSkin was also cut into small pieces. The pieces from the human skin and LabSkin were washed three times with washing buffer and centrifuged at 50 *g* for 10 minutes. Samples were incubated overnight at 4 ºC with 10 mL lysis buffer (25 mM Tris pH 7.6, 150 mM sodium chloride, 1% NP40, 0.5% sodium deoxycholate, 0.1% SDS, 1 mM EDTA) incorporating enzymatic inhibitor (Roche, UK). Samples were homogenised using a mechanical device (Ultra Turrax T25) using 10 cycles of 30 seconds interspersed with 30 seconds resting time on ice between cycles. After this procedure, the homogenate was centrifuged at 9,000 *g* for 30 minutes at 4 ºC, and the supernatant was collected in a clean tube and clarified using DNAse. Therefore, the protein sample extracted using this strategy are representative of total cellular protein.

Protein digestion

Protein content in the LabSkin and human skin samples was estimated by a spectrophotometric protein assay using Bradford reagent (ThermoFisher Scientific, Hemel Hempstead, UK) (Bradford, 1976). Analysis was made in triplicate according to the manufacturer's protocol using bovine serum albumin (BSA) as a standard. Based on the results of the Bradford assay, 100 µg of each fraction was spiked with an internal standard protein mixture containing 17 pmol equine myoglobin, 12 pmol bovine cytochrome *c* and 3 pmol BSA. These non-human proteins were selected because their low similarity

with their human counterparts minimises interference. To each fraction containing the standards, sodium deoxycholate was added to achieve a final concentration of 10% (w/v). The mixture was mixed well and incubated at room temperature for 10 minutes. The filter-aided sample preparation (FASP) method was used as previously described (Al Feteisi *et al.*, 2018; Couto *et al.*, 2019). Disulfide bridges were reduced by adding 100 mM (final concentration) 1,4-dithiothreitol (DTT) and thiols were alkylated by adding 50 mM (final concentration) iodoacetamide. After alkylation and three washes with 1M urea in 50 mM ammonium bicarbonate (pH 8.5), protein digestion was performed by adding trypsin (trypsin:protein ratio 1:25 w/w) followed by overnight incubation at 37°C. Peptides were recovered by centrifugation (14,000 *g,* 20 minutes) first by elution using 100 mM ammonium bicarbonate (pH 8.5) followed by a second elution using 0.5 M sodium chloride. A desalt process was performed using a C18 column (Nest group, USA) as previously described (Couto *et al*., 2019). The peptides were dried using a vacuum concentrator and stored at -20°C until mass spectrometric analysis.

Liquid chromatography and mass spectrometry (LC-MS)

Dried peptides samples were resuspended in 100 µL loading buffer [97% (v/v) HPLC water, 3% (v/v) HPLC acetonitrile and 0.1% (v/v) trifluoracetic acid] and 1.0 µL of each sample was loaded in duplicate on an UltiMate® 3000 rapid separation liquid chromatograph (RSLC) (Dionex, Surrey, UK) coupled to an on-line Q Exactive™ HF Hybrid Quadrupole-Orbitrap™ Mass Spectrometer (ThermoFisher Scientific, Bremen, Germany). Peptides were reversed-phase separated on a PepMap™ RSLC C18 column (2 µm particles, 100 Å, 75 µm inner diameter, 50 cm length) (Thermo Scientific, UK) preceded by a C18 PepMap100 µ-precolumn (5 µm, 100 Å, 5 µm inner diameter, 5 mm length) (ThermoFisher Scientific, UK). A multi-step gradient was used from 4% to 40% buffer B (80% (v/v) acetonitrile with 0.1% (v/v) formic acid) for 100 minutes at a flow rate of 300 nL min^{-1}. The composition of buffer A was HPLC grade water containing 0.1 % (v/v) formic acid. The sensitivity and m/z accuracy of the mass

spectrometer was evaluated using a positive ion calibration solution (ThermoFisher Scientific, Paisley, UK). The performance of the liquid chromatography and mass spectrometer was evaluated using HeLa protein digest standard (ThermoFisher Scientific, Paisley, UK) over a 90 minutes gradient. Data were acquired in the positive ion mode in a data-dependent manner alternating between survey MS and MS/MS scans. MS scans were performed over the range of 100−1500 m/z, at 60,000 resolution, automatic gain control (AGC) of 3×10^6, and 100 ms maximal injection time. The top 18 precursor ions were sequentially selected for fragmentation using higher-energy collisional dissociation (HCD) with 28% normalized collision energy and precursor isolation window of 1.2 m/z. MS/MS scans were acquired at 30,000 resolution, AGC of 5×10^4 and 120 ms maximal injection time. Dynamic exclusion was set to 30 s.

Data analysis for label-free quantification of proteins

Protein/peptide identification was performed using MaxQuant. Proteins were identified by searching against a reference human proteome database containing 71,599 entries (UniProt, May 2017). Using MaxQuant, the precursor mass tolerance was set to 5 ppm, fragment mass tolerance was set to 0.02 Da, cysteine carbamidomethylation was considered as fixed modification and oxidation of methionine and deamidation of asparagine/glutamine were considered as variable modifications. Trypsin was set as the proteolytic enzyme and one missed cleavage was allowed. Based on ion intensity, protein quantification was manually calculated using myoglobin as standard. From the three standards, myoglobin proved to be the one that generated at least two reliable unique peptides. Peptide uniqueness and absence of missed cleavages were required for quantification purposes.

Assessment of protein subcellular localization, molecular function and composition of skin samples

To assess differences in the make-up of the human skin and LabSkin, the sub-cellular localization of all identified proteins (*n* = 3030, 1749 and 1463, respectively) was annotated according to three databases: Gene Ontology (GO), UniProt and the Human Protein Atlas (HPA), by searching the gene names against these repositories. In addition, the PANTHER (Protein ANalysis THrough Evolutionary Relationships) classification system version 14.0 (http://www.pantherdb.org/) was used to assign protein functional class. Markers for different cell types in the skin epidermis (keratinocytes, Langerhans cells) and different sub-layers (stratum spinosum, stratum granulosum and stratum corneum) were identified using HPA and UniProt databases.

Statistical analysis

All statistical analysis of the data was performed using Microsoft Excel 2010 and GraphPad Prism® v7.04 (La Jolla California, USA). Abundance data of proteins in human skin samples are represented as mean ± standard deviation (SD), median, range and coefficient of variation (CV). Figures were generated using GraphPad Prism® v7.04.

Matrix-assisted laser desorption ionization mass spectrometry imaging (MALDI-MSI)

Sample preparation

Terbinafine hydrochloride, tolbutamide, methylphenidate hydrochloride and ritalinic acid were made up as 0.5 % (w/v) solutions in an emulsion of 80:20 (v/v) water:olive oil with 10% (v/v) isosorbide dimethyl ether (DMI) and 20 µL of each solution was topically applied on LabSkin in triplicate. Treated LabSkin

was incubated at 37 °C for 24 hours. After incubation, LabSkin was washed with HPLC-grade ethanol to remove excess formulation and, then snap-frozen with liquid nitrogen cooled isopentane (2-5 minutes) and stored at - 80 °C. For cryosectioning, the LabSkin sections were transferred into a Cryostat (Leica 200 UV, Leica Microsystems, Milton Keynes, UK), mounted onto a cork ring using distilled water at −25 °C for 30 minutes to allow thermal equilibration. Tissue sections were cryosectioned at 12 µm, thaw mounted onto polylysine-coated glass slides, and stored at -80 °C.

Sublimation

Three hundred milligrams of matrix α-cyano-4-hydroxycinnamic acid was spread evenly at the bottom of the sublimation apparatus (Sigma Aldrich, Gillingham, UK). Polylysine glass slides contain LabSkin tissue sections were attached to the flat top of the chamber. The flat top of the chamber was then attached to the bottom using an O-ring seal and vacuum was applied. When a stable vacuum of 2.5 x 10^{-2} Torr was achieved, the top was filled with cold water (5 °C) and the temperature was set up at 180 °C. The sublimation process was performed until the optimal amount of α-cyano-4-hydroxycinnamic acid (between 0.1 and 0.2 mg cm^{-2}) was achieved. Following sublimation, a recrystallisation step was performed.

MALDI mass spectrometry imaging

Tissues sections of LabSkin treated with terbinafine hydrochloride and tolbutamide were imaged using a Bruker Autoflex III fitted with a “Smartbeam” Nd:YAG laser (355 nm, 1 kHz) (Bruker, Bremen, Germany) at a spatial resolution 50 µm x 50 µm, at a range of 100 - 1500 m/z. The tissues sections of LabSkin treated with methylphenidate hydrochloride were imaged using a Synapt™ G2 (Waters, Manchester, UK) in full scan sensitivity mode at a range of 100 - 1500 m/z with a resolution 10,000 full

width at half maximum at a spatial resolution of 60 µm x 60 µm, and with laser energy set to 250 arbitrary units. The ion mobility function of the instrument was not enabled. All images were acquired in positive ion mode. MALDI-MSI data for LabSkin tissue sections treated with terbinafine hydrochloride and tolbutamide were processed using the FlexAnalysis software (Bruker Daltonics, Bremen, Germany). MALDI-MSI data for LabSkin tissue sections treated with methylphenidate hydrochloride were processed using HDI 1.4 mass spectrometry imaging software (Waters, Manchester, UK).

Results

A label-free global quantitative proteomic analysis of 6 human skin samples and two independent replicates of LabSkin samples was carried out, with a particular focus on the analysis of xenobiotic metabolizing enzymes and transporters (phase I, II and III) and other enzymes (redox enzymes, peptidases and peptidases inhibitors, and endonucleases) that support xenobiotic metabolism in skin. We identified and quantified approximately 2000 proteins in both human skin and LabSkin from which 78 XMEs including some auxiliary enzymes and transporters (Tables 2, 3 and 4), 36 redox enzymes (Table 5) and 60 enzymes (Table 6) belonging to the peptidase family, nuclease family and peptidases inhibitors family were quantified. MALDI imaging was used to validate the label-free proteomics data, particularly with regard to CYP and esterase presence.

Evaluation of protein subcellular localization, molecular function and composition of skin samples

The number of proteins quantified in human skin was higher (n = 3030) than in LabSkin replicate 1 (n = 1749) (hereafter called LabSkin 1) and LabSkin replicate 2 (n = 1463) (hereafter called LabSkin 2). The localization and functional assignment of proteins identified in human skin samples and LabSkin replicates are shown in Figure 1. Localization (Figure 1A) and functional analysis (Figure 1C) reflected

differences between human skin and LabSkin, with an overlap of about 32% (Figure 1B). An analysis of cellular markers was performed using the proteomics data. Human skin showed markers for both keratinocytes (CALML5, KRT19) and Langerhans cells (CD207) whereas LabSkin contained markers for keratinocytes only. Markers for layers of epidermis were found in both human skin and LabSkin, including stratum spinosum markers (KRT10, CASP14), stratum granulosum marker (FLG) and stratum corneum marker (KLK5), although LabSkin 2 lacked detectable stratum corneum markers. A schematic representation of the different layers and cell types of the epidermis is shown in Figure 2. In general, the abundance of all quantified markers were expressed at higher levels in human skin, followed by LabSkin 1 and then LabSkin 2 (Table 1).

Abundance of XME and transporters

We were able to quantify a variety of proteins with known roles in phase I, phase II and phase III drug/xenobiotic metabolism from the total cellular protein extract (Figure 3). Table 2 and Figure 3A provide quantitative information regarding phase I XME in human skin and LabSkin. The most abundant phase I XMEs in human skin sections were alcohol dehydrogenase 1B, ADH1B (23.39 ± 14.12 pmol mg^{-1}), alcohol dehydrogenase 1C, ADH1C (37.46 ± 15.05 pmol mg^{-1}), aldehyde dehydrogenase 1, ALDH1A1 (21.01 ± 6.70 pmol mg^{-1}) and carbonyl reductase 1, CBR1 (25.30 ± 6.99 pmol mg^{-1}). These enzymes were also quantified as highly abundant enzymes in LabSkin although ADH1C and ALDH1A1 were absent in LabSkin 1.

Cytochrome P450 enzymes are especially prevalent in the liver (Couto *et al.*, 2019; El-Khateeb *et al.*, 2019), and to a lesser extent the intestine (Couto *et al.*, 2020). In the skin only three cytochrome P450 enzymes, namely CYP51A1 (0.98 ± 0.09 pmol mg^{-1}), CYP7B1 (2.57 ± 0.45 pmol mg^{-1}) and CYP8A1 (5.52 ± 4.70 pmol mg^{-1}) were identified and quantified. These enzymes were also quantified in LabSkin

1 where they were present in approximately similar abundance to that in human skin, but not in LabSkin 2. A similar trend was observed with the auxiliary proteins for CYPs including cytochrome b5, CYB5A (9.54 ± 5.15 pmol mg^{-1}), NADPH-cytochrome P450 reductase, POR (4.46 ± 0.77 pmol mg^{-1}) and several isoforms of NADH-cytochrome b5 reductase (CYB5R1/R2/R3). These proteins were only quantified in human skin and LabSkin 1 as shown in Table 2.

Three alcohol dehydrogenases and several aldehyde dehydrogenase isoforms were found in high abundance in human skin (Table 2). Alcohol dehydrogenases convert alcohols into aldehydes or ketones. Of the three alcohol dehydrogenases quantified, ADH1B and ADH5 were quantified in human skin and LabSkin. Although ADH5 has previously been reported in skin at the protein level, ADH1B has previously been observed only as mRNA (Uhlen *et al.*, 2015). In addition to these, ADH1C was quantified for the first time in human skin and in LabSkin 2. Aldehyde dehydrogenases are involved in the oxidation of a plethora of aldehyde groups to carboxylates, and were expressed with similar abundance in LabSkin and human skin. We have quantified ALDH1L2 in human skin at the protein level for the first time, although the corresponding mRNA level has previously been observed (Uhlen *et al.*, 2015).

A number of reductases were quantified including several isoforms of the aldo-keto reductase family, two carbonyl reductase isoforms and biliverdin reductase A (BLVRA). The aldo-keto reductases AKR1A1, AKR1B1 and AKR1C2 have previously been reported in human skin only at the level of mRNA while AKR1D1 has not previously been reported in any form (Uhlen *et al.*, 2015). Biliverdin reductase (BLVRA) and the carbonyl reductases were found at similar levels in LabSkin compared to human skin whereas the aldo-keto reductases were predominantly expressed at lower levels.

Other phase I enzymes quantified are shown in Table 2. Examples include amine oxidases (AOC2, AOC3), aldehyde oxidase AOX1, carboxylesterase CES1, epoxide hydrolase EPHX1/2 and leukotriene A4 hydrolase LTA4H. In general (80% of the quantified other phase I enzymes) human skin and LabSkin 1 showed similar levels of these enzymes, but the abundances of a large proportion of these proteins (50%) were lower in LabSkin 2 compared to human skin. AOC2, MAOA and VKORC1 were quantified in human skin but not in LabSkin.

The phase II XME identified and quantified in the human skin and LabSkin are shown in Table 3 and Figure 3B. These include glutathione-S-transferases, sulfotransferases and other transferases. In contrast with the human liver, no uridine 5'-diphospho-glucuronosyltransferase (UGT) enzymes were identified in these samples indicating that glucuronidation plays a minor role in skin while glutathionation and sulfonation are important reactions in the metabolism of several xenobiotics and drugs (Couto *et al.*, 2019). From all phase II enzymes identified and quantified, GSTP1 (π) is the most abundant with concentration 62.65 ± 17.78 pmol mg^{-1} protein, followed by GSTM4 (μ) and GSTM3 (μ) with concentrations of 21.75 ± 0.63 pmol mg^{-1} protein and 19.68 ± 10.29 pmol mg^{-1} protein, respectively. These three enzymes have previously been reported only at the level of mRNA (Uhlen *et al.*, 2015). Amongst glutathione-S-transferases, 45% of the enzymes (4 out of 9) quantified in human skin were quantified in LabSkin 1 and 78% of the enzymes (7 out of 9) quantified in the human skin were also quantified in LabSkin 2. LabSkin 2 contains almost all the glutathione-S-transferases found in skin, but often at reduced concentrations. In LabSkin 1, fewer glutathione-S-transferases were detected, but their concentrations fell within the range found in human skin. In stark contrast to glutathione-S-transferases, sulfotransferases were not detected in LabSkin despite the quantification of these enzymes in the human skin sections. The occurrence of MAT1A (5.36 ± 1.87 pmol mg^{-1}) is a new finding, not previously reported in human skin (Uhlen *et al.*, 2015). Among the seven other transferases

detected in the human skin, four were quantified in LabSkin 1 and six were quantified in LabSkin 2. The abundance of two proteins, COMT and NNMT were higher in LabSkin 1 compared to human skin. The abundance of all six quantified proteins in LabSkin 2 was within the range quantified in human skin. Thiopurine S-methyltransferase, TPMT, was below the limit of quantification in LabSkin and this enzyme was only quantified in 2 out of 6 human skin samples.

Only few phase III transporters were found in our skin samples and they were generally low abundance as shown in Table 4 and Figure 3C. Of the ABC transporters, only ABCA8 and ABCB11 were securely quantified in the human skin, but ABCA8 could not be detected in LabSkin. Amongst the eight SLC transporters quantified in human skin, less than 50% were quantified in LabSkin and they were generally found in lower abundance compared to human skin.

Assessment of the abundance of enzymes with a supportive role in xenobiotic metabolism - redox enzymes

Phase II XME are typically involved in detoxification of a wide variety of highly reactive intermediate substrates formed in phase I. Therefore, redox enzymes such as catalase (CAT), glutathione synthetase (GSS), and peroxiredoxins are typically categorised as phase II XME (van Eijl *et al.*, 2012). As shown in Table 5, human skin and LabSkin are very rich in redox enzymes. We identified and quantified a plethora of redox enzymes such as catalase, superoxide dismutases, thioredoxins and glutaredoxins. Thioredoxin, TXN, was the most abundant in human skin (84.87 ± 20.01 pmol mg^{-1}) followed by peroxiredoxin 1, PRDX1, (53.52 ± 11.78 pmol mg^{-1}). Both were found in high abundance in both LabSkin replicates. Also highly abundant in both human skin and LabSkin (> 20 pmol mg^{-1}) were superoxide dismutases (SOD1/2/3), peroxiredoxins (PRDX2/5/6), prolyl 4-hydroxylase (P4HB) and disulfide-isomerases (PDIA3/6). Amongst GPX enzymes, GPX3 enzyme was the most abundant in

human skin (19.57 ± 13.60 pmol mg^{-1}) but GPX3/4 was absent in LabSkin. All three naturally found SOD isoforms were identified and quantified in human skin and their abundance followed the rank order SOD3 > SOD1 > SOD2. SOD3 is also known as extracellular superoxide dismutase [Cu-Zn] and its abundance in human skin was in the range of 40.85 ± 19.72 pmol mg^{-1} protein. Although all SOD isoforms were found in LabSkin, their abundance and rank order were different to those found in human skin. We also identified and quantified the seleno proteins GPX4 (8.97 ± 2.24 pmol mg^{-1} protein) and TXNRD1 (4.61 ± 1.51 pmol mg^{-1} protein) known for their important antioxidant role in the human skin. These enzymes have been reported to be the two most abundant seleno proteins expressed in the skin epidermis and cultured keratinocytes (Sengupta *et al.*, 2010).

Assessment of the abundance of enzymes with a supportive role in xenobiotic metabolism – peptidases and nucleases.

Proteolytic enzymes and their inhibitors are highly represented in skin and they represent more than 2% of the human genome (Puente *et al.*, 2005). Therefore, it is not surprising that proteases/peptidases and their inhibitors have an essential role in controlling multiple biological processes, including xenobiotic metabolism (Craik *et al.*, 2011). Proteases and protease inhibitors work together to control development and maturation of keratinocytes in the epidermis (Zeeuwen, 2004). Proteases from the serine, metallo, aspartic and cysteine categories were identified and quantified in both human skin and LabSkin, as shown in Table 6. In human skin, the most abundant peptidases/proteases was dermicidin, DCD (30.98 ± 20.58 pmol mg^{-1} protein), and was expressed in similar abundance in LabSkin 2. This protein was found in low abundance in LabSkin 1. The second most abundant protein in human skin was cathepsin D, CTSD (24.35 ± 6.18 pmol mg^{-1} protein). This enzyme was also quantified in LabSkin at similar levels. The most abundant peptidase/protease inhibitors were cystatin-B, CSTB (42.93 ± 22.3 pmol mg^{-1} protein), which was expressed at similar

levels in both human skin and LabSkin and plasma protease C1 inhibitor SERPING1 (24.68 ± 6.61 pmol mg^{-1} protein) which was much less abundant in LabSkin compared with the human skin.

Assessment of CYP and esterase activity in LabSkin by substrate based MALDI imaging

From the results of the label-free quantitative proteomics, CYP enzymes were almost absent in human skin and LabSkin, with only CYP51A1, CYP7B1 and CYP8A1 quantified in human skin at less than 5 pmol mg^{-1} protein. In contrast, enzymes with potential esterase activity such as PON1 (11.28 ± 1.99 pmol mg^{-1} total protein), CES1 (14.43 ± 1.91 pmol mg^{-1} total protein) and ESD (15.15 ± 3.72 pmol mg^{-1} total protein) were quantified at abundance levels equivalent to a majority of the XME in human skin and LabSkin. MALDI-MSI experiments were performed to examine the CYP and esterase activity in LabSkin using the substrate-based mass spectrometry imaging (SB-MSI) approach. To examine CYP activity, LabSkin tissue was treated with terbinafine, a substrate for CYP2C9, CYP1A2, and CYP3A4, and tolbutamide, a CYP2C9 substrate, prior to SB-MSI. No metabolite formation was observed, indicating the absence of CYP2C9, CYP1A2 and CYP3A4 activity in the human skin (Figure 4). This is in agreement with the label-free quantitative proteomics data in which these enzymes were not identified or quantified. To examine esterase activity, LabSkin was treated with 0.5% (w/w) of hCES1 substrate methylphenidate hydrochloride for 24 hours. Figure 5 shows MALDI-MSI images of the distribution of methylphenidate ion at *m/z* 234 and the metabolite, ritalinic acid ion at *m/z* 220 in both blank and treated LabSkin sections recorded at 60 µm spatial resolution. It can be seen that the metabolite ritalinic acid signal appeared to be localised in the outer layer of skin i.e. epidermis.

Discussion

In Europe, although animal testing of cosmetic ingredients has been discontinued, topical drugs are still tested on animals and there is clearly a need for alternative model systems to assess the safety and

efficacy of both topical drugs and cosmetic ingredients. Although several artificial human skin models have been proposed, they are limited by a lack of understanding of xenobiotic metabolism and transport in human skin. Efforts have been made to understand XME gene expression in human skin and *in vitro* skin models using reverse transcription polymerase chain reaction (Kazem *et al.*, 2019); however, it is increasingly accepted that mRNA abundance is a poor proxy for protein abundance and activity (Maier *et al.*, 2009; Couto *et al.*, 2020). In this study, we used a combination of label-free quantitative mass spectrometry and substrate-based mass spectrometry imaging to assess xenobiotic metabolism in human skin and an *in vitro* artificial skin model (LabSkin) and have quantified several XMEs for the first time in these systems.

Xenobiotic metabolism is divided into three phases; oxidation (phase I), addition of polar groups to phase I metabolites (phase II), and clearance from cells (phase III). A single, pioneering mass spectrometry-based study on xenobiotic metabolism in skin, focuses on phase I and phase II enzymes only (van Eijl *et al.*, 2012). We have now quantified phase I and phase II enzymes and also transporters and accessory enzymes involved in xenobiotic metabolism using mass spectrometry.

In the liver, phase I metabolism is dominated by enzymes from the CYP family (Couto *et al.*, 2019), but there is disagreement about the importance of CYP enzymes in skin (van Eijl *et al.*, 2012; Kazem *et al.*, 2019). We have identified three CYP enzymes, CYP7B1, CYP8A1 and CYP51A1, primarily involved in endogenous metabolism. CYP enzymes with a known role in xenobiotic metabolism, such as CYP1A2, CYP2C9 and CYP3A4, were neither identified nor quantified. Substrate-based mass spectrometry imaging confirmed the absence of the activity of these CYP enzymes in LabSkin. This observation agrees with previous studies by mass spectrometry-based proteomics and Western blots where the enzymes from CYP families 1, 2, 3 and 4 were not detected (van Eijl *et al.*, 2012). Conventionally, CYP activity in human skin has been assessed by either 7-ethoxy resorufin O-

deethylase (EROD) assay for CYP1 enzymes, 7-methoxy-4-(trifluoromethyl)-coumarin O-demethylase (MFCOD) assay for CYP2 enzymes or the benzyloxy-4-trifluoromethylcoumarin-O-debenzy-loxylase (BFCOD) assay for CYP3 enzymes. These studies reported either activity close to the limit of detection or below the limit of detection (Kazem *et al.*, 2019). mRNA transcripts of CYP enzymes have, however, been quantified in native human skin, suggesting that CYP expression may be regulated at the level of protein translation. It has been suggested that certain CYP enzymes are induced in the presence of specific substrates (Ahmad and Mukhtar, 2004). By contrast with human skin, CYP activity has been established conclusively in the skin of mouse models (Oesch *et al.*, 2014), indicating that animal models may have limited applicability to human products. With regard to the LabSkin assessed in this study, the protein abundance of CYP and auxiliary proteins in LabSkin 1 were comparable to *ex vivo* human skin whilst no CYP enzymes were detected in LabSkin 2.

Other phase I xenobiotic metabolising enzymes: dehydrogenases, reductases, esterases and hydrolases, were quantified in our study. Although the abundance of these proteins have not been previously measured, the presence of these proteins in native human skin has been previously reported (van Eijl *et al.*, 2012). Carboxylesterase activity has not been previously demonstrated in human skin in spite of the quantification of the cognate mRNA in HaCaT keratinocytes and skin models (Kazem *et al.*, 2019). We quantified CES1 and CES1P1 in human skin. Although, the abundance of these enzymes was lower in LabSkin, substrate-based mass spectrometry imaging was used to evaluate CES1 activity for the first time, and indeed, CES1 activity was found in LabSkin.

The important role of protein glutathionylation in skin is highlighted by the identification and quantification of several GSTs isoforms among phase II xenobiotic metabolising enzymes. GST activity in human skin has been confirmed in previous studies using a broad spectrum GST substrate as well as through gene expression and proteomic studies (van Eijl *et al.*, 2012; Kazem *et al.*, 2019). In

agreement with previous studies, GST pi was the most abundant GST enzyme in our study. Reversible protein glutathionylation is known to play a role in cellular regulation, signalling transduction and antioxidant defense (Dalle-Donne *et al.*, 2007; Gallogly and Mieyal, 2007). Moreover, glutathione conjugates may be further processed and secreted and further metabolism occurs extracellularly (Couto *et al.*, 2016). We also quantified sulfotransferase enzymes in the human skin explants, which were not detected previously (van Eijl *et al.*, 2012). Whilst SULTs are absent in mouse skin, they are essential for the metabolism of endogenous compounds in humans (Oesch *et al.*, 2014; Kazem *et al.*, 2019). The abundance of GST isoforms and other transferase enzymes in LabSkin were similar to native human skin. SULT enzymes were not detected in LabSkin. The abundance of SULT mRNA has been observed to increase upon calcium-induced differentiation of human keratinocytes (Oesch *et al.*, 2018). Therefore, our inability to detect SULTs in the LabSkin models may be linked to the *in vitro* culturing conditions. Evidence for the presence of mRNA of SULT enzymes and SULT activity in human skin has been reported (Kazem *et al.*, 2019). We were also able to confidently quantify catechol-O-methyltransferase (COMT) for the first time.

Although mRNA of UGT and NAT enzymes have been quantified in low abundance in human skin, our results agree with previous proteomics studies where these enzymes were not detected in human skin (van Eijl *et al.*, 2012). Conflicting observations between activity assays, mRNA abundance and proteomics studies may be because these enzymes are preferentially expressed in certain human anatomical sites or because the expression of these proteins are controlled at the level of protein translation. More studies are needed to shed light on the role of regulatory cellular processes in human skin.

The use of unbiased, label free, quantitative proteomics approach to lysates of epidermal cells and LabSkin provided us with an opportunity to detect and quantify transporter proteins. Although the use

of membrane-based protein preparations would enable a comprehensive insight into the transporters in the human skin epidermis; using our total cellular protein extract, we were able to confidently quantify two ABC and 8 SLC transporters, presumably those of highest abundance. The mRNA abundance of certain ABC and SLC transporters has been quantified in human keratinocytes and *ex vivo* human skin (Osman-Ponchet *et al.*, 2014; Fujiwara *et al.*, 2015). The mRNA transcripts of ABCC3 has been established to be the highest is human skin, although large interindividual variability is reported amongst the Caucasian population (Takechi *et al.*, 2018). We did not detect ABCC3 in our study but found good evidence of ABCA8 and ABCB11. Similarly, the mRNA transcripts of SLC22A3 and SLCO3A1 have been established to be the highest in human skin (Takechi *et al.*, 2018) but we detected neither SLC22A3 nor SLCO3A1 at the protein level. ABCA8 is known to be involved in ATP-dependent lipophilic drug transport (Tsuruoka *et al.*, 2002) and ABCB11 is involved in the secretion of conjugated bile salts (Hayashi *et al.*, 2005). The SLC transporter proteins detected in the human skin in our study are associated with endogenous metabolism and some play important roles in skin conditions (Nakamura *et al.*, 2010; Gomez *et al.*, 2013). SLC25A5 is known to be highly expressed in psoriasis compared with normal skin (Lundberg *et al.*, 2015) and SLC12A2 may be involved in transport of fumaric acid esters used to treat psoriasis (Onderdijk *et al.*, 2014). SLC12A2 has been quantified for the first time in this study. In LabSkin, apart from SLC25A6 and SLC44A1, the abundance of transporters was low and in some cases undetected.

The label-free approach also allowed us to quantify antioxidant enzymes in human skin and LabSkin. Antioxidant enzymes play an important auxiliary role in xenobiotic metabolism as they sequester the reactive oxygen species produced during phase I xenobiotic metabolism (Couto *et al.*, 2016) but are not routinely investigated when studying xenobiotic metabolism. To our knowledge, the abundance of antioxidant enzymes in skin, liver and kidney has not been reported to date. We contend that

incorporation of the analysis of antioxidants and antioxidant enzymes when studying xenobiotic metabolism is important. Xenobiotic metabolism has the potential to upset the fine redox balance maintained in human skin and lead to skin conditions such as psoriasis, atopic dermatitis and cancer (Ben-Yehuda Greenwald *et al.*, 2016; Couto *et al.*, 2016). Our results indicate that the human skin contains a high diversity and abundance of redox enzymes, which can be mimicked in LabSkin.

We hypothesise that proteases and peptidases also play an important role in maintaining cellular homeostasis in skin exposed to xenobiotics, by regulating phase I enzymes, phase II enzymes, transporters and redox enzymes. Indeed, dysregulation of proteases and peptidases in human skin is known to affect skin hydration and maintenance of skin integrity (Verdier-Sévrain and Bonté, 2007). Moreover, bioactive peptides and proteins are increasingly employed in topical drugs and cosmetics and the presence and activity of proteases and peptidases in skin can alter the lifespan of these additives in topical drugs and cosmetics. To our knowledge, this is the first report of the abundance of proteases and peptidases in human skin and the most abundant proteases and peptidases in human skin were also detected in LabSkin.

Although a wide variety of XMEs, transporters and auxiliary proteins were quantified in human skin, high interindividual variability was seen in the presence and abundance of these proteins across the six samples used in this study (columns 2 and 3 in Tables 2 - 6). The modest number (n=6) of human skin samples studied here precludes a deeper analysis of the reasons underlying the high interindividual variability. Such high interindividual variability in XME and transporter abundance has also been reported in mass spectrometry-based quantitative proteomics studies of human liver and intestine (Couto *et al.*, 2019, 2020). A similarly high interbatch variability is seen across the two independent replicates of LabSkin. Despite this, predominantly, proteins that were present in all six human skin samples were also found in both replicates of LabSkin. Interbatch differences observed in LabSkin may

be due to differences in the level of differentiation of keratinocytes at the point of analysis. For example, LabSkin 2 lacked detectable stratum corneum markers suggesting that it may have had a more immature phenotype than LabSkin 1. However, a larger study involving a greater number of LabSkin batches and a greater number of human skin samples will allow a better understanding of the sources of interbatch and interindividual variability.

In conclusion, we report for the first time, the protein abundance of XMEs, transporters and auxiliary enzymes involved in xenobiotic metabolism in human skin and LabSkin. Improved understanding of skin physiology will aid validation of *in vitro* living skin equivalents and the development of robust mathematical models that can be used to predict drug metabolism and disposition in human skin. The *in vitro* living skin equivalent model, LabSkin, evaluated in this study was shown to express a number of proteins present in human skin. Whilst the abundance of some of these proteins are equivalent to skin, a few proteins are either not detected or have low abundance. The data in our study can guide the refinement of culturing conditions to ensure that the proteomic profile of LabSkin is representative of *in vivo* human skin in order to confidently reduce, refine and replace the use of animals in development of safe and efficacious topical drugs and cosmetics. In particular, we anticipate that the inclusion of the abundance of redox enzymes and proteases and peptidases in mathematical models will enable such models to become more robust and representative of xenobiotic metabolism in human skin.

Acknowledgements

The authors thank the National Centre for the Replacement, Refinement and Reduction of Animals in Research (NC3Rs) for funding this work through the Metaboderm CRACK IT challenge. The authors also thank the ChELSI Institute, University of Sheffield, for access to LC-MS/MS instrumentation

(funded under BBSRC grant: BB/M012166/1; and EPSRC grant:EP/E036252/1). Cristina Russo thanks Croda Ltd for funding her PhD.

Author contributions

Participated in research design: Couto, Newton, Sidaway, Rostami-Hodjegan, Clench, Barber.

Conducted experiments: Couto, Newton, Russo, Karunakaran, Al-Majdoub.

Contributed new reagents or analytical tools: Couto, Russo.

Performed data analysis: Couto, Newton, Russo, Karunakaran, Achour.

Wrote or contributed to the writing of the manuscript: Couto, Karunakaran, Newton, Russo, Achour, Sidaway, Rostami-Hodjegan, Clench, Barber.

Conflict of interests

The authors declare no competing financial interest.

References

Ahmad N, and Mukhtar H (2004) Cytochrome P450: A Target for Drug Development for Skin Diseases. *J Invest Dermatol* **123**:417–425.

Al Feteisi H, Al-Majdoub ZM, Achour B, Couto N, Rostami-Hodjegan A, and Barber J (2018) Identification and quantification of blood-brain barrier transporters in isolated rat brain microvessels. *J Neurochem* **146**:670–685.

Ben-Yehuda Greenwald M, Ben-Sasson S, Bianco-Peled H, and Kohen R (2016) Skin Redox Balance

Maintenance: The Need for an Nrf2-Activator Delivery System. *Cosmetics* **3**:1.

Bradford MM (1976) A rapid and sensitive method for the quantitation of microgram quantities of protein utilizing the principle of protein-dye binding. *Anal Biochem* **72**:248–254.

Cantòn I, Cole DM, Kemp EH, Watson PF, Chunthapong J, Ryan AJ, MacNeil S, and Haycock JW (2010) Development of a 3D human in vitro skin co-culture model for detecting irritants in real-time. *Biotechnol Bioeng* **106**:794–803.

Chau DYS, Johnson C, MacNeil S, Haycock JW, and Ghaemmaghami AM (2013) The development of a 3D immunocompetent model of human skin. *Biofabrication* **5**:035011.

Couto N, Al-Majdoub ZM, Achour B, Wright PC, Rostami-Hodjegan A, and Barber J (2019) Quantification of Proteins Involved in Drug Metabolism and Disposition in the Human Liver Using Label-Free Global Proteomics. *Mol Pharm* **16**:632–647.

Couto N, Al-Majdoub ZM, Gibson S, Davies PJ, Achour B, Harwood MD, Carlson G, Barber J, Rostami-Hodjegan A, and Warhurst G (2020) Quantitative Proteomics of Clinically Relevant Drug-Metabolizing Enzymes and Drug Transporters and Their Intercorrelations in the Human Small Intestine. *Drug Metab Dispos* **48**:245–254.

Couto N, Malys N, Gaskell SJ, and Barber J (2013) Partition and turnover of glutathione reductase from saccharomyces cerevisiae: A proteomic approach. *J Proteome Res* **12**.

Couto N, Wood J, and Barber J (2016) The role of glutathione reductase and related enzymes on cellular redox homoeostasis network. *Free Radic Biol Med* **95**:27–42.

Craik CS, Page MJ, and Madison EL (2011) Proteases as therapeutics. *Biochem J* **435**:1–16.

Dalle-Donne I, Rossi R, Giustarini D, Colombo R, and Milzani A (2007) S-glutathionylation in protein redox regulation. *Free Radic Biol Med* **43**:883–898.

El-Khateeb E, Vasilogianni A-M, Alrubia S, Al-Majdoub ZM, Couto N, Howard M, Barber J, Rostami-Hodjegan A, and Achour B (2019) Quantitative mass spectrometry-based proteomics in the era of model-informed drug development: Applications in translational pharmacology and recommendations for best practice. *Pharmacol Ther* 107397, Elsevier Inc.

Flores C, Santos M, Pereira SB, Mota R, Rossi F, De Philippis R, Couto N, Karunakaran E, Wright PC, Oliveira P, and Tamagnini P (2019) The alternative sigma factor SigF is a key player in the control of secretion mechanisms in Synechocystis sp. PCC 6803. *Environ Microbiol* **21**:343–359.

Fujiwara R, Takenaka S, Hashimoto M, Narawa T, and Itoh T (2015) Expression of human solute carrier family transporters in skin: possible contributor to drug-induced skin disorders. *Sci Rep* **4**:5251.

Gallogly MM, and Mieyal JJ (2007) Mechanisms of reversible protein glutathionylation in redox signaling and oxidative stress. *Curr Opin Pharmacol* **7**:381–391.

Gomez G, Nardone V, Lotfi-Emran S, Zhao W, and Schwartz LB (2013) Intracellular Adenosine Inhibits IgE-Dependent Degranulation of Human Skin Mast Cells. *J Clin Immunol* **33**:1349–1359.

Hayashi H, Takada T, Suzuki H, Onuki R, Hofmann A, and Sugiyama Y (2005) Transport by vesicles of glycine- and taurine-conjugated bile salts and taurolithocholate 3-sulfate: A comparison of human BSEP with rat Bsep. *Biochim Biophys Acta - Mol Cell Biol Lipids* **1738**:54–62.

Hu J, Van den Steen PE, Sang Q-XA, and Opdenakker G (2007) Matrix metalloproteinase inhibitors as

therapy for inflammatory and vascular diseases. *Nat Rev Drug Discov* **6**:480–498.

Kazem S, Linssen EC, and Gibbs S (2019) Skin metabolism phase I and phase II enzymes in native and reconstructed human skin: a short review. *Drug Discov Today* **24**:1899–1910.

Lundberg KC, Fritz Y, Johnston A, Foster AM, Baliwag J, Gudjonsson JE, Schlatzer D, Gokulrangan G, McCormick TS, Chance MR, and Ward NL (2015) Proteomics of Skin Proteins in Psoriasis: From Discovery and Verification in a Mouse Model to Confirmation in Humans. *Mol Cell Proteomics* **14**:109–119.

Maier T, Güell M, and Serrano L (2009) Correlation of mRNA and protein in complex biological samples. *FEBS Lett* **583**:3966–3973.

Mathes SH, Ruffner H, and Graf-Hausner U (2014) The use of skin models in drug development. *Adv Drug Deliv Rev* **69**–**70**:81–102.

Nakamura T, Fujiwara R, Ishiguro N, Oyabu M, Nakanishi T, Shirasaka Y, Maeda T, and Tamai I (2010) Involvement of Choline Transporter-Like Proteins, CTL1 and CTL2, in Glucocorticoid-Induced Acceleration of Phosphatidylcholine Synthesis via Increased Choline Uptake. *Biol Pharm Bull* **33**:691–696.

Oesch F, Fabian E, Guth K, and Landsiedel R (2014) Xenobiotic-metabolizing enzymes in the skin of rat, mouse, pig, guinea pig, man, and in human skin models. *Arch Toxicol* **88**:2135–2190.

Oesch F, Fabian E, and Landsiedel R (2018) Xenobiotica-metabolizing enzymes in the skin of rat, mouse, pig, guinea pig, man, and in human skin models. *Arch Toxicol* **92**:2411–2456.

Onderdijk AJ, Balak DMW, Baerveldt EM, Florencia EF, Kant M, Laman JD, IJcken WFJ, Racz E,

Ridder D, Thio HB, and Prens EP (2014) Regulated genes in psoriatic skin during treatment with fumaric acid esters. *Br J Dermatol* **171**:732–741.

Osman-Ponchet H, Boulai A, Kouidhi M, Sevin K, Alriquet M, Gaborit A, Bertino B, Comby P, and Ruty B (2014) Characterization of ABC transporters in human skin. *Drug Metabol Drug Interact* **29**.

Overall CM, and Dean RA (2006) Degradomics: Systems biology of the protease web. Pleiotropic roles of MMPs in cancer. *Cancer Metastasis Rev* **25**:69–75.

Parker JL, Lowry RC, Couto NAS, Wright PC, Stafford GP, and Shaw JG (2014) Maf-dependent bacterial flagellin glycosylation occurs before chaperone binding and flagellar T3SS export. *Mol Microbiol* **92**:258–272.

Puente XS, Sánchez LM, Gutiérrez-Fernández A, Velasco G, and López-Otín C (2005) A genomic view of the complexity of mammalian proteolytic systems. *Biochem Soc Trans* **33**:331–334.

Raut MP, Couto N, Karunakaran E, Biggs CA, and Wright PC (2019) Deciphering the unique cellulose degradation mechanism of the ruminal bacterium Fibrobacter succinogenes S85. *Sci Rep* **9**:16542.

Russo C, Brickelbank N, Duckett C, Mellor S, Rumbelow S, and Clench MR (2018) Quantitative Investigation of Terbinafine Hydrochloride Absorption into a Living Skin Equivalent Model by MALDI-MSI. *Anal Chem* **90**:10031–10038.

Russo DA, Couto N, Beckerman AP, and Pandhal J (2016) A Metaproteomic Analysis of the Response of a Freshwater Microbial Community under Nutrient Enrichment. *Front Microbiol* **7**.

Sengupta A, Lichti UF, Carlson BA, Ryscavage AO, Gladyshev VN, Yuspa SH, and Hatfield DL (2010)

Selenoproteins Are Essential for Proper Keratinocyte Function and Skin Development. *PLoS One* **5**:e12249.

Takechi T, Hirota T, Sakai T, Maeda N, Kobayashi D, and Ieiri I (2018) Interindividual Differences in the Expression of ATP-Binding Cassette and Solute Carrier Family Transporters in Human Skin: DNA Methylation Regulates Transcriptional Activity of the Human ABCC3 Gene. *Drug Metab Dispos* **46**:628–635.

Tsuruoka S, Ishibashi K, Yamamoto H, Wakaumi M, Suzuki M, Schwartz GJ, Imai M, and Fujimura A (2002) Functional analysis of ABCA8, a new drug transporter. *Biochem Biophys Res Commun* **298**:41–45.

Uhlen M, Fagerberg L, Hallstrom BM, Lindskog C, Oksvold P, Mardinoglu A, Sivertsson A, Kampf C, Sjostedt E, Asplund A, Olsson I, Edlund K, Lundberg E, Navani S, Szigyarto CA-K, Odeberg J, Djureinovic D, Takanen JO, Hober S, Alm T, Edqvist P-H, Berling H, Tegel H, Mulder J, Rockberg J, Nilsson P, Schwenk JM, Hamsten M, von Feilitzen K, Forsberg M, Persson L, Johansson F, Zwahlen M, von Heijne G, Nielsen J, and Ponten F (2015) Tissue-based map of the human proteome. *Science (80-)* **347**:1260419–1260419.

van Eijl S, Zhu Z, Cupitt J, Gierula M, Götz C, Fritsche E, and Edwards RJ (2012) Elucidation of Xenobiotic Metabolism Pathways in Human Skin and Human Skin Models by Proteomic Profiling. *PLoS One* **7**:e41721.

Verdier-Sévrain S, and Bonté F (2007) Skin hydration: a review on its molecular mechanisms. *J Cosmet Dermatol* **6**:75–82.

Zeeuwen PLJM (2004) Epidermal differentiation: The role of proteases and their inhibitors. *Eur J Cell*

Biol **83**:761–773.

Figure legends

Figure 1 – Localization and functional assignment of proteins identified in human skin and two independent replicates of LabSkin. Protein localization (A) was based on gene ontology (GO), Uniprot and Human Protein Atlas (HPA) databases. Overlaps between the proteins identified in human skin and LabSkin are outlined in the Venn diagram (B). Functional classes were assigned using the PANTHER database (C). Proteins relevant to membrane traffic and metabolizing enzymes are highlighted. Panel D shows cellular and epidermis regional markers. Cellular markers include those specific for keratinocytes (CALML5, KRT19) and Langerhans cells (CD207). Makers for layers of the epidermis include those specifically expressed in the stratum spinosum (KRT10, CASP14), stratum granulosum (FLG) and stratum corneum (KLK5). Markers were confirmed using Uniprot and HPA databases. PM, plasma membrane; ER, endoplasmic reticulum; n, number of proteins.

Figure 2 – Schematic representation of the layers of thin human skin epidermis. From the deep to the superficial layer, the epidermis consists of stratum basale, stratum spinosum, stratum granulosum and stratum corneum. In thick human skin, a discernible fifth layer (not represented here) called stratum lucidum is present between the stratum granulosum and stratum corneum. Epidermis is mostly composed of keratinocytes. Melanocytes and Merkel cells are present in low abundance in the stratum basale, and Langerhans cells are predominantly present in low abundance in the stratum spinosum.

Figure 3 – The protein quantities of epidermal enzymes and transporters expressed in human skin and LabSkin. Phase I enzymes (A) include cytochrome P450 monooxygenases, dehydrogenases, reductases and hydrolases. Phase II enzymes (B) are involved in conjugation reactions and include glutathione -S- transferases and sulfotransferases. Phase III proteins are transporters which include ATP-binding cassette (ABC) transporters and solute carriers (SLC).

Figure 4 – MALDI MSI on a LabSkin section treated with terbinafine (A) and tolbutamide (B). Terbinafine is a substrate for CYP2C9, CYP1A2, and CYP3A4. No evidence of metabolite formation was observed in terbinafine-treated LabSkin section (purple) (A). Tolbutamide is a substrate for CYP2C9. The tolbutamide is shown in green and PC Lipid Head Group is shown in red. No evidence of metabolite formation was observed (B). Arrow indicates a magnified image.

Figure 5 – MALDI MSI on a LabSkin section treated with methylphenidate (0.5% w/w) for 24 hours showing the distribution of A) methylphenidate peak at m/z 234; B) ritalinic acid peak at m/z 220. Untreated LabSkin (blank) sections were included as controls (left) alongside methylphenidate-treated LabSkin section (middle). Standard ritalinic acid (top) and methylphenidate (bottom) were spotted at a concentration of 1 mg mL^{-1} alongside the LabSkin sections as can be seen towards the left of the images. MS images clearly show presence of the substrate, methylphenidate, in the epidermis (A) and the presence of the product of esterase activity, ritalinic acid, in the epidermis (B).

Tables

Table 1 – Expression levels of cellular markers including those specific for keratinocytes and Langerhans cells. Identified makers for layers of the epidermis include proteins specifically expressed in the stratum spinosum, stratum granulosum and stratum corneum. Protein identification and quantification was based on the presence of at least 2 unique peptides and from human skin in at least two donors. Protein expression is represented by the mean, the standard deviation of the mean (SD), the coefficient of variation (%CV). The range of protein expression (min – max) and the number of samples (n) are also reported. Protein abundance is reported in pmol mg^{-1} of protein.

	Human Skin			*LabSkin 1*	*LabSkin 2*
Protein	***Mean ± SD (CV)***	***Range (n)***	***Median***		
Keratinocyte markers					
CALML5	67.65 ± 16.50 (24.39)	39.29 – 88.07 (6)	72.23	63.10	56.92
KRT19	14.56 ± 3.99 (27.41)	13.20 – 16.99 (6)	14.36	4.75	10.30
Langerhans cell marker					
CD207	8.53 ± 0.77 (9.02)	7.98 – 9.06 (2)	8.52		
Epidermis markers - stratum spinosum					
KRT10	4.85 ± 2.14 (44.20)	1.87 – 8.17 (6)	4.86	2.66	2.91
CASP14	16.29 ± 2.88 (17.70)	11.82 – 18.99 (6)	17.68	15.16	12.76
Epidermis markers - stratum granulosum					
FLG	4.18 ± 1.73 (41.39)	1.93 – 5.86 (6)	4.51	2.80	1.36
Epidermis markers - stratum corneum					
KLK5	7.27 ± 2.86 (39.43)	6.54 – 8.00 (2)	7.27	2.47	

Table 2 – Expression levels of phase I xenobiotic metabolising enzymes in human skin and LabSkin. Protein identification and quantification was based on the presence of at least 2 different peptides and from human skin of at least two donors. Protein expression is represented by the mean, the standard deviation of the mean (SD), the coefficient of variation (%CV). The range of protein expression (min – max) and the number of samples (n) are also reported. Protein abundance is reported in pmol mg^{-1} of protein.

	Human Skin			*LabSkin 1*	*LabSkin 2*
Protein	***Mean ± SD (CV)***	***Range (n)***	***Median***		
Cytochrome P450 and auxiliary proteins					
CYP51A1*	0.98 ± 0.09 (9.38)	0.92 – 1.05 (2)	0.98	1.19	
CYP7B1	2.57 ± 0.45 (17.43)	2.26 – 2.89 (2)	2.57	3.50	
CYP8A1 (PTGIS)	5.52 ± 4.70 (91.25)	1.58 – 12.73 (4)	3.88	2.60	
POR	4.46 ± 0.77 (17.16)	3.66 – 5.19 (3)	4.54	3.21	
CYB5A	9.54 ± 5.15 (54.02)	3.26 – 15.45 (6)	10.56	6.52	
CYB5R1	11.31 ± 6.05 (53.55)	7.02 – 15.59 (2)	11.31	2.06	
CYB5R2*	5.93 ± 2.02 (34.00)	3.5 – 8.58 (5)	5.31	3.55	
CYB5R3	10.27 ± 2.57 (25.05)	6.98 – 13.05 (6)	10.66	20.75	
Dehydrogenases					
ADH1B*	23.39 ± 14.12 (60.39)	4.01 – 48.02 (6)	21.60	13.86	22.40
ADH1C**	37.46 ± 15.05 (40.16)	13.80 – 55.35 (5)	39.01		32.53
ADH5	18.81 ± 7.96 (42.32)	4.73 – 29.04 (6)	19.38	18.30	9.08
ALDH16A1	5.23 ± 1.74 (33.32)	3.41 – 6.88 (3)	5.39		
ALDH1A1	21.01 ± 6.70 (31.86)	11.88 – 28.84 (5)	21.35		12.13
ALDH1B1	2.59 ± 1.09 (42.19)	1.71 – 3.82 (5)	1.90	6.09	
ALDH1L1	3.93 ± 1.53 (38.85)	2.40 – 5.45 (3)	3.95	4.93	
ALDH1L2*	4.09 ± 1.52 (37.27)	3.01 – 5.17 (2)	4.09	7.55	
ALDH2	17.48 ± 7.75 (44.32)	5.31 – 25.01 (6)	19.97	6.64	12.54

ALDH3A1	4.45 ± 1.60 (36.01)	2.76 – 6.12 (5)	4.56		8.08
ALDH3A2	2.67 ± 0.43 (15.93)	2.22 – 3.28 (6)	2.55	3.39	1.77
ALDH4A1	3.10 ± 0.33 (10.78)	2.72 – 3.31 (3)	3.28	2.95	1.97
ALDH6A1	4.27 ± 1.07 (25.06)	2.48 – 5.82 (6)	4.33	3.46	1.65
BDH2	6.13 ± 3.46 (56.51)	3.68 – 8.58 (2)	6.13	3.03	
Reductases					
AKR1A1*	14.39 ± 2.68 (18.65)	11.39 – 17.98 (6)	14.43	6.30	7.82
AKR1B1*	6.87 ± 2.74 (39.85)	2.59 – 9.66 (5)	6.89	3.63	4.93
AKR1C1	7.35 ± 2.91 (39.57)	4.21 – 11.62 (6)	6.73		6.53
AKR1C2*	6.70 ± 2.17 (32.32)	3.90 – 9.31 (6)	6.33	4.03	4.11
AKR1C3	12.42 ± 5.60 (45.07)	4.41 – 18.98 (6)	14.11	5.41	7.37
AKR1D1**	15.03 ± 7.06 (46.99)	7.52 – 25.89 (5)	13.12	1.90	19.60
AKR7A2	8.01 ± 1.32 (16.51)	7.08 – 8.95 (2)	8.01	6.88	
BLVRA	6.75 ± 2.34 (34.70)	3.92 – 9.36 (5)	6.12	4.56	4.27
CBR1	25.30 ± 6.99 (27.62)	12.44 – 31.51 (6)	27.96	16.56	27.73
CBR3	9.00 ± 1.32 (14.62)	7.45 – 10.44 (5)	9.59	9.20	9.93
Others					
AOC2*	10.59 ± 7.54 (71.21)	3.49 – 21.26 (4)	8.81		
AOC3*	15.72 ± 4.86 (30.94)	11.20 – 23.83 (6)	14.22		5.89
AOX1	3.00 ± 1.18 (39.26)	1.65 – 3.84 (3)	3.52		3.55
CES1*	14.43 ± 1.91 (13.23)	11.70 – 16.21 (5)	14.73		6.29
CES1P1**	16.32 ± 6.34 (38.87)	12.27 – 27.45 (5)	14.37	3.07	10.52
CRYZ	6.89 ± 2.20 (31.90)	2.43 – 8.08 (6)	7.70	6.46	4.49
DHRS7	4.16 ± 3.36 (80.81)	0.92 – 7.62 (3)	3.93	5.93	
DPYD*	1.98 ± 1.06 (53.73)	0.94 – 3.07 (3)	1.94	1.28	
EPHX1*	10.00 ± 5.06 (50.63)	4.17 – 15.57 (6)	9.91	11.84	4.97
EPHX2	6.57 ± 0.51 (7.73)	6.21 – 6.93 (2)	6.57		6.49
ESD	15.15 ± 3.72 (24.58)	9.29 – 18.38 (6)	17.00	12.18	9.69
LTA4H	9.85 ± 3.07 (31.16)	5.00 – 14.29 (6)	9.57	7.15	8.13
PIN1*	12.10 ± 4.51 (37.26)	8.25 – 18.63 (4)	10.77		6.71
PON1	11.28 ± 1.99 (17.64)	8.32 – 13.81 (5)	11.20		6.61
YWHAH	7.23 ± 1.57 (21.67)	4.92 – 9.00 (6)	7.08	5.69	7.33
MAOA	7.16 ± 7.03 (98.27)	2.18 – 12.13 (2)	7.16		
PTGES3***	17.62 ± 4.70 (26.69)	12.87 – 21.73 (4)	17.95	8.95	
PTGS1 (COX-1)	3.93 ± 0.06 (1.41)	3.89 – 3.97 (2)	3.93	10.88	
VKORC1****	12.14 ± 13.00 (107.12)	2.94 – 21.34 (2)	12.14		

* - according to Human Protein Atlas, these enzymes are reported to be present in the skin at the RNA level (low copy numbers) but not at the protein level. ** - according to Human Protein Atlas, these enzymes are not reported to be present in the skin at the RNA or protein level. *** - This is a nuclear receptor. **** - Warfarin targets this enzyme therefore interfering with blood coagulation in humans.

Table 3 – Expression levels of phase II xenobiotic-metabolizing enzymes in human skin and LabSkin. Protein identification and quantification was based on the presence of at least 2 different peptides and from human skin of at least two donors. Protein expression is represented by the mean, the standard deviation of the mean (SD), the coefficient of variation (%CV). The range of protein expression (min – max) and the number of samples (n) are also reported. Protein abundance is reported in pmol mg^{-1} of protein.

	Human Skin			*Lab Skin 1*	*Lab Skin 2*
Protein	***Mean ± SD (CV)***	***Range (n)***	***Median***		
Glutathione transferases					
GSTK1 (kappa)	9.99 ± 3.26 (32.67)	6.47 – 15.24 (6)	9.05	18.99	6.73
GSTM2 (mu)	9.59 ± 4.07 (42.47)	2.47 – 14.72 (6)	10.00		14.11
GSTM3 (mu)*	19.68 ± 10.29 (52.29)	4.91 – 31.93 (6)	22.90	8.83	22.90
GSTM4 (mu)	21.75 ± 0.63 (2.91)	21.28 – 22.47 (3)	21.51		
GSTM5 (mu)*	12.24 ± 5.33 (43.54)	6.59 – 19.44 (4)	11.47		5.94
GSTO1 (omega)	9.59 ± 3.43 (35.72)	4.75 – 13.71 (6)	9.04	8.94	7.83
GSTP1 (pi)	62.65 ± 17.78 (28.38)	39.31 – 82.46 (6)	60.22	82.10	30.45
GSTT1 (theta)	18.84 ± 3.31 (17.56)	16.50 – 21.17 (3)	18.84		7.31
MGST1	11.26 ± 9.94 (88.27)	2.69 – 22.16 (3)	8.93		
Sulfo-transferases					
SULT1A4*	4.08 ± 0.40 (9.73)	3.84 – 4.54 (3)	3.87		
SULT2B1	3.98 ± 2.21 (55.61)	2.42 – 5.55 (2)	3.98		
Other transferases					
COMT	10.13 ± 2.84 (28.06)	5.31 – 13.25 (6)	10.58	29.74	11.12
MAT1A**	5.36 ± 1.87 (34.97)	2.19 – 7.71 (6)	5.48	4.25	4.57
MPST	3.97 ± 2.44 (61.52)	1.21 – 5.86 (3)	4.84		4.45
NNMT	6.01 ± 3.03 (50.43)	2.74 – 8.73 (3)	6.57	15.47	5.65
TGM3	4.83 ± 0.95 (19.73)	3.81 – 5.70(3)	4.99		3.35
TPMT	3.27 ± 0.22 (6.73)	3.11 – 3.42 (2)	3.27		

TST	3.36 ± 1.81 (53.86)	1.66 – 6.44 (5)	2.82	5.20	3.08

* - according to Human Protein Atlas, these enzymes are reported to be present in the skin at the RNA level (low copy numbers) but not at the protein level. ** - according to Human Protein Atlas, these enzymes are not reported to be present in the skin at the RNA or protein level.

Table 4 – Expression levels of phase III xenobiotic transporters in human skin and LabSkin. Protein identification and quantification was based on the presence of at least 2 different peptides and from human skin of at least two donors. Protein expression is represented by the mean, the standard deviation of the mean (SD), the coefficient of variation (%CV), the range (min – max) and the number of samples (n). Protein abundance is reported in pmol mg^{-1} of protein.

	Human Skin			*Lab Skin 1*	*Lab Skin 2*
Protein	***Mean ± SD (CV)***	***Range (n)***	***Median***		
ATP binding cassette					
ABCA8	2.92 ± 0.97 (33.10)	2.24 – 3.60 (2)	2.92		
ABCB11**	7.90 ± 2.03 (25.64)	5.39 – 10.05 (4)	8.09	4.99	4.81
Solute carriers					
SLC12A2	3.31 ± 0.80 (24.24)	2.43 – 4.52 (5)	3.07		2.10
SLC25A3*	4.92 ± 1.85 (37.65)	2.98 – 7.23 (4)	4.74	2.84	
SLC25A5	5.50 ± 1.27 (23.00)	4.61 – 6.40 (2)	5.50		
SLC25A6	3.50 ± 1.79 (51.19)	1.46 – 4.82 (3)	4.21	4.16	
SLC29A1	5.77 ± 0.79 (13.70)	5.21 – 6.32 (2)	5.77		
SLC44A1*	3.75 ± 2.24 (59.81)	2.29 – 6.34 (3)	2.63	3.62	
SLC44A2*	4.71 ± 1.89 (40.22)	3.37 – 6.04 (2)	4.71		
SLC4A1**	4.94 ±0.92 (18.64)	4.22 – 6.20 (4)	4.67		1.65

* - according to Human Protein Atlas, these transporters are reported to be present in the skin at the RNA level (low copy numbers) but not at the protein level. ** - according to Human Protein Atlas, these transporters are not reported to be present in the skin at the RNA or protein level.

Table 5 – Expression levels of enzymes in human skin and LabSkin with a role in oxidative stress and xenobiotic metabolism. Protein identification and quantification was based on the presence of at least 2 different peptides and from human skin of at least two donors. Protein expression is represented by the mean, the standard deviation of the mean (SD), the coefficient of variation (%CV), the range (min – max) and the number of samples (n). Protein abundance is reported in pmol mg^{-1} of protein.

	Human Skin			*Lab Skin 1*	*Lab Skin 2*
Protein	***Mean ± SD (CV)***	***Range (n)***	***Median***		
Catalase					
CAT*	13.63 ± 4.38 (32.15)	7.78 – 18.40 (6)	14.30	6.37	8.49
Superoxide dismutases					
SOD1	24.99 ± 5.16 (20.66)	19.61 – 31.52 (6)	23.36	12.35	33.59
SOD2	22.99 ± 15.88 (69.07)	10.48 – 54.23 (6)	19.53	67.11	13.45
SOD3	40.85 ± 19.72 (48.28)	6.22 – 62.05 (6)	42.87	9.29	20.39
CCS	3.61 ± 1.04 (28.73)	2.88 – 5.08 (4)	3.24		2.56
Glutathione peroxidases					
GPX1	8.59 ± 0.96 (11.12)	7.56 – 10.04 (5)	8.69		5.99
GPX3	19.57 ± 13.60 (69.50)	7.32 – 38.04 (5)	13.28		
GPX4	8.97 ± 2.24 (24.96)	6.61 – 12.08 (5)	9.01		
Glutaredoxins					
GLRX*	16.93 ± 6.71 (39.62)	11.70 – 24.49 (3)	14.59	12.39	6.36
GLRX3	3.92 ± 0.13 (3.26)	3.83 – 4.01 (2)	3.92		2.58
Thioredoxins					
TXNRD1	4.61 ± 1.51 (32.84)	3.53 – 6.81 (4)	4.05	1.43	5.41
TXN	84.87 ± 20.01 (23.58)	61.22 – 112.57 (6)	86.32	59.33	80.07
TXN2	7.68 ± 2.77 (36.10)	4.13 – 11.07 (5)	7.52		5.51
TXNL1	6.84 ± 2.16 (31.59)	3.39 – 9.65 (6)	6.89	3.83	4.65
TXNDC5	9.50 ± 2.07 (21.82)	6.83 – 12.48 (6)	9.25	23.71	6.87
TXNDC12*	3.95 ± 0.52 (13.06)	3.36 – 4.58 (4)	3.93	3.01	
TXNDC17	11.56 ± 3.09 (26.70)	7.78 – 16.83 (6)	11.09	14.28	8.88

TMX1	11.48 ± 1.75 (15.25)	10.24 – 12.71 (2)	11.48	7.16	
Glutathione metabolism					
GSR	8.74 ± 2.16 (24.70)	5.36 – 11.35 (5)	9.06	4.89	5.03
GSS	6.33 ± 1.93 (30.57)	4.32 – 9.07 (6)	6.06	5.99	3.79
HAGH	3.52 ± 1.99 (56.66)	1.78 – 6.31 (4)	3.00		
GLO1*	15.44 ± 5.66 (36.68)	6.60 – 21.43 (6)	17.18	12.45	14.59
Peroxiredoxins					
PRDX1	53.52 ± 11.78 (22.01)	30.73 – 64.38 (6)	56.35	66.81	63.62
PRDX2	34.70 ± 3.60 (10.37)	27.95 – 38.49 (6)	35.49	27.12	36.83
PRDX3	17.67 ± 2.50 (14.18)	14.14 – 21.48 (6)	17.48	28.16	10.99
PRDX4	7.55 ± 2.96 (39.20)	3.81 – 11.92 (6)	6.96	37.50	4.57
PRDX5	26.93 ± 4.86 (18.05)	18.85 – 31.72 (6)	28.55	18.77	23.50
PRDX6	34.29 ± 6.64 (19.36)	22.85 – 39.92 (6)	36.96	23.23	33.52
FAM213A	16.63 ± 7.25 (43.62)	8.04 – 24.01 (5)	18.57		6.70
Methanethiol oxidase					
SELENBP1*	15.45 ± 2.16 (13.98)	12.52 – 17.52 (5)	15.61	6.67	12.30
Disulfide-isomerases					
P4HB	26.09 ± 6.99 (26.77)	19.16 – 37.98 (6)	24.39	51.53	14.86
PDIA3	21.82 ± 8.73 (40.01)	11.87 – 37.20 (6)	20.28	40.86	12.07
PDIA4	7.17 ± 1.43 (19.89)	4.98 – 8.66 (6)	7.62	9.31	4.35
PDIA6	22.34 ± 11.09 (49.63)	11.67 – 42.56 (6)	19.33	46.98	12.22
Scavenger receptors					
SSC5D	5.30 ± 2.61 (49.26)	2.26 – 8.82 (5)	5.00	4.16	
CD163**	9.16 ± 3.71 (40.52)	4.61 – 12.83 (5)	10.57		4.79

* - according to Human Protein Atlas, these enzymes are reported to be present in the skin at the RNA level (low copy numbers) but not at the protein level. ** - according to Human Protein Atlas, these enzymes are not reported to be present in the skin at the RNA or protein level.

Table 6 – Expression levels of proteases, nucleases and protease inhibitors in human skin and LabSkin. Protein identification and quantification was based on the presence of at least 2 different peptides and from human skin of at least two donors. Protein expression is represented by the mean, the standard deviation of the mean (SD), the coefficient of variation (%CV), the range (min – max) and the number of samples (n). Protein abundance is reported in pmol mg^{-1} of protein.

	Human Skin			*Lab Skin 1*	*Lab Skin 2*
Protein	***Mean ± SD (CV)***	***Range (n)***	***Median***		
Aminopeptidases					
ANPEP*	13.03 ± 10.09 (77.39)	5.48 – 27.33 (4)	9.66	22.74	
DNPEP	9.93 ± 2.47 (24.83)	7.10 – 11.58 (3)	11.12		1.51
ERAP1	4.63 ± 1.09 (23.55)	2.91 – 5.88 (6)	4.92	5.35	3.36
LAP3	10.14 ± 4.56 (44.94)	4.59 – 16.93 (6)	9.77	6.95	5.36
LNPEP	6.42 ± 2.40 (37.42)	4.72 – 8.12 (2)	6.42		
METAP1	3.10 ± 0.66 (21.19)	2.63 – 3.56 (2)	3.10	9.24	1.68
NPEPPS*	7.99 ± 1.51 (18.92)	5.91 – 9.61 (6)	8.05	9.51	5.76
RNPEP	19.51 ± 28.19 (144.45)	5.60 – 76.85 (6)	8.54	42.01	71.51
XPNPEP1	3.90 ± 1.70 (43.57)	2.40 – 6.32 (4)	3.44	5.41	
XPNPEP3	8.34 ± 0.50 (5.99)	7.77 – 8.67 (3)	8.58		5.38
Endopeptidases					
ASPRV1	11.12 ± 2.94 (26.47)	6.18 – 14.54 (6)	11.26	30.14	7.58
CAPN1	12.54 ± 2.14 (17.04)	10.63 – 15.72	11.85	12.61	9.86
CAPN2	9.99 ± 2.57 (25.73)	5.94 – 12.85 (5)	10.42	5.45	8.25
FAP	4.50 ± 1.44 (31.93)	2.93 – 5.76 (3)	4.80	5.14	
PREP	6.28 ± 1.76 (28.06)	4.51 – 8.83 (6)	5.89	5.15	3.64
Peptidases/Proteases					
CNDP2	11.59 ± 3.45 (29.76)	5.16 – 15.59 (6)	12.17	5.45	8.23
DPP3	4.94 ± 1.88 (38.15)	2.98 – 8.06 (5)	4.59	5.69	3.61
DPP4*	4.80 ± 2.00 (41.63)	2.99 – 7.65 (4)	4.28	6.17	
DPP7	2.81 ± 1.78 (63.27)	1.55 – 4.06 (2)	2.81	3.30	
LONP1	4.51 ± 0.99 (21.85)	3.40 – 5.29 (3)	4.85	5.70	1.95
PEPD	6.22 ± 1.85 (29.75)	3.78 – 8.71 (6)	6.45	3.81	5.21
TPP1	10.57 ± 2.27 (21.50)	7.48 – 13.66 (5)	10.52	12.08	5.66

CTSA	5.26 ± 2.30 (43.64)	2.28 – 8.60 (5)	4.75	14.37	3.06
CTSB	8.95 ± 2.56 (28.54)	4.49 – 11.53 (6)	9.70	9.27	5.03
CTSC	7.72 ± 4.41 (57.13)	5.41 – 15.59 (5)	5.84	20.44	2.73
CTSD	24.35 ± 6.18 (25.38)	17.65 – 32.76	23.59	19.12	11.39
CTSG**	9.50 ± 6.73 (70.84)	4.74 – 14.26 (2)	9.50		2.51
CTSZ	8.06 ± 3.12 (38.75)	4.25 – 12.62 (5)	8.27	16.80	3.60
DCD***	30.98 ± 20.58 (66.44)	10.73 – 60.60	20.73	4.53	49.02
BLMH	7.08 ± 2.22 (31.36)	5.75 – 9.65 (3)	5.86		
Metalloproteases					
ADAM10	3.13 ± 0.55 (17.46)	2.75 – 3.52 (2)	3.13		
MMP2*	4.99 ± 5.49 (110.16)	1.10 – 8.87 (2)	4.99	8.08	
Carboxypeptidases					
CPA3*	9.56 ± 4.67 (48.82)	4.59 – 15.00 (4)	9.33		
CPB2**	5.63 ± 1.79 (31.83)	2.91 – 7.90 (5)	5.92		2.98
CPM*	3.89 ± 1.60 (41.09)	2.76 – 5.02 (2)	3.89		
CPN1**	10.13 ± 2.23 (21.98)	8.56 – 11.71 (2)	10.13		
CPN2**	6.93 ± 1.36 (19.60)	4.66 – 8.11 (5)	7.13		2.45
CPQ*	3.92 ± 1.04 (26.49)	2.69 – 5.38 (5)	4.07	4.63	2.28
CPVL*	2.85 ± 0.92 (32.30)	1.98 – 3.82 (3)	2.75		
PRCP	4.79 ± 2.27 (47.45)	2.97 – 9.20 (6)	4.13	10.76	
Nucleases					
ENDOD1	4.57 ± 2.66 (58.22)	2.18 – 7.48 (4)	4.30	4.08	
RNASE1*	9.46 ± 1.79 (18.87)	7.54 – 11.64 (5)	8.80		
RNASE4*	3.78 ± 1.98 (52.39)	1.41 – 6.22 (4)	3.74		3.14
RNASET2	6.57 ± 1.39 (21.14)	4.58 – 7.65 (4)	7.03	5.55	
SND1	3.43 ± 2.35 (68.57)	1.38 – 7.44 (5)	2.79	9.25	
TATDN1	5.55 ± 2.21 (39.73)	2.54 – 7.49 (4)	6.09		
YBX1****	2.73 ± 1.43 (52.45)	1.22 – 4.50 (4)	2.60	5.55	
Peptidase/Protease inhibitors					
CST3	9.88 ± 3.61 (36.54)	6.07 – 14.71 (5)	9.58	18.39	6.21
CST6	8.66 ± 3.01 (34.80)	5.58 – 12.82 (5)	8.42		
CSTA	9.24 ± 5.47 (59.24)	5.37 – 13.10 (2)	9.24	15.59	
CSTB	42.93 ± 22.3 (52.0)	25.65 – 82.24	34.01	38.07	37.26
PI16	8.74 ± 2.83 (32.37)	5.61 – 13.24 (5)	7.84		4.24
SERPING1*	24.68 ± 6.61 (26.79)	13.15 – 29.79	26.39	3.26	13.21
SPINK5	7.06 ± 2.02 (28.64)	5.63 – 8.49 (2)	7.06	3.96	
Proteosome					
PSMC1	6.89 ± 1.04 (15.02)	6.16 – 7.62 (2)	6.89	1.82	

PSMC2	2.61 ± 0.96 (36.79)	1.24 – 3.42 (4)	2.88	4.25	1.78
PSMC3	5.22 ± 1.45 (27.83)	3.38 – 7.74 (6)	5.02	5.86	3.24
PSMC5	2.95 ± 0.86 (29.03)	1.69 – 3.59 (4)	3.26	4.41	
PSMC6	3.80 ± 1.09 (28.76)	2.82 – 5.53 (5)	3.54	6.66	1.99
Ribonuclease inhibitor					
RNH1	22.47 ± 5.55 (24.71)	12.60 – 25.88	24.34	21.65	17.56

* - according to Human Protein Atlas, these enzymes are reported to be present in the skin at the RNA level (low copy numbers) but not at the protein level. ** - according to Human Protein Atlas, these enzymes are not reported to be present in the skin at the RNA or protein level. *** - Also displays antimicrobial activity thereby limiting skin infection by potential pathogens in the first few hours after bacterial colonization. **** - YBX1 can promotes the expression of multidrug resistance 1 (MDR1) gene, which is involved in the development of drug resistance.

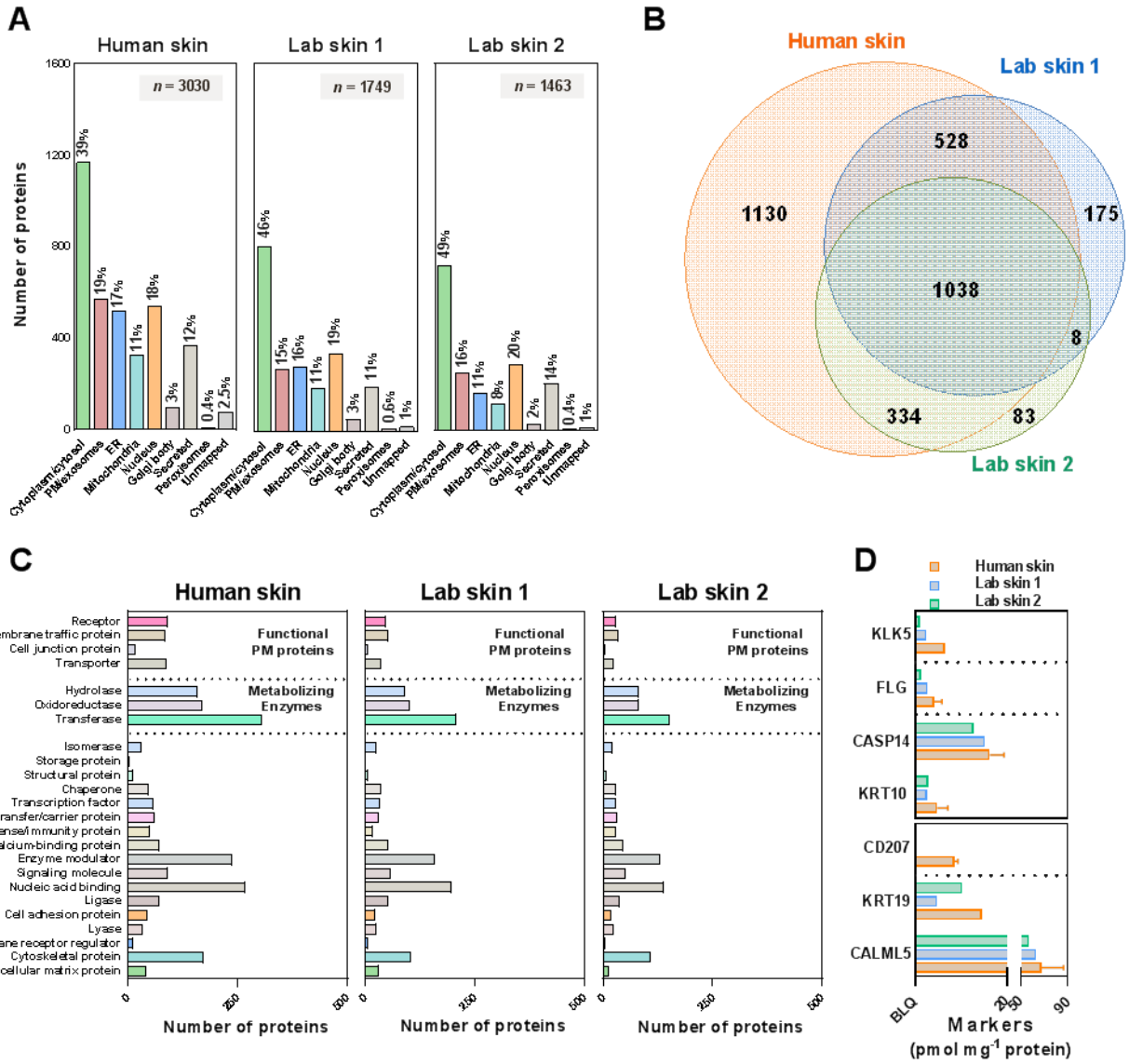
A
Human skin
Lab skin 1
Lab skin 2
n = 3030
n = 1749
n = 1463
Number of proteins
1600
1200
800
400
0
39%
19%
17%
11%
18%
3%
12%
0.4%
2.5%
46%
15%
16%
11%
19%
3%
11%
0.6%
1%
49%
16%
11%
8%
20%
2%
14%
0.4%
1%
Cytoplasm/cytosol
PM/exosomes
ER
Mitochondria
Nucleus
Golgi body
Secreted
Peroxisomes
Unmapped
B
Human skin
Lab skin 1
Lab skin 2
528
1130
175
1038
8
334
83
C
Human skin
Lab skin 1
Lab skin 2
Functional PM proteins
Metabolizing Enzymes
Receptor
Membrane traffic protein
Cell junction protein
Transporter
Hydrolase
Oxidoreductase
Transferase
Isomerase
Storage protein
Structural protein
Chaperone
Transcription factor
Transfer/carrier protein
Defense/immunity protein
Calcium-binding protein
Enzyme modulator
Signaling molecule
Nucleic acid binding
Ligase
Cell adhesion protein
Lyase
Transmembrane receptor regulator
Cytoskeletal protein
Extracellular matrix protein
0
250
500
Number of proteins
D
Human skin
Lab skin 1
Lab skin 2
KLK5
FLG
CASP14
KRT10
CD207
KRT19
CALML5
BLQ
20
250
90
Markers
(pmol mg-1 protein)

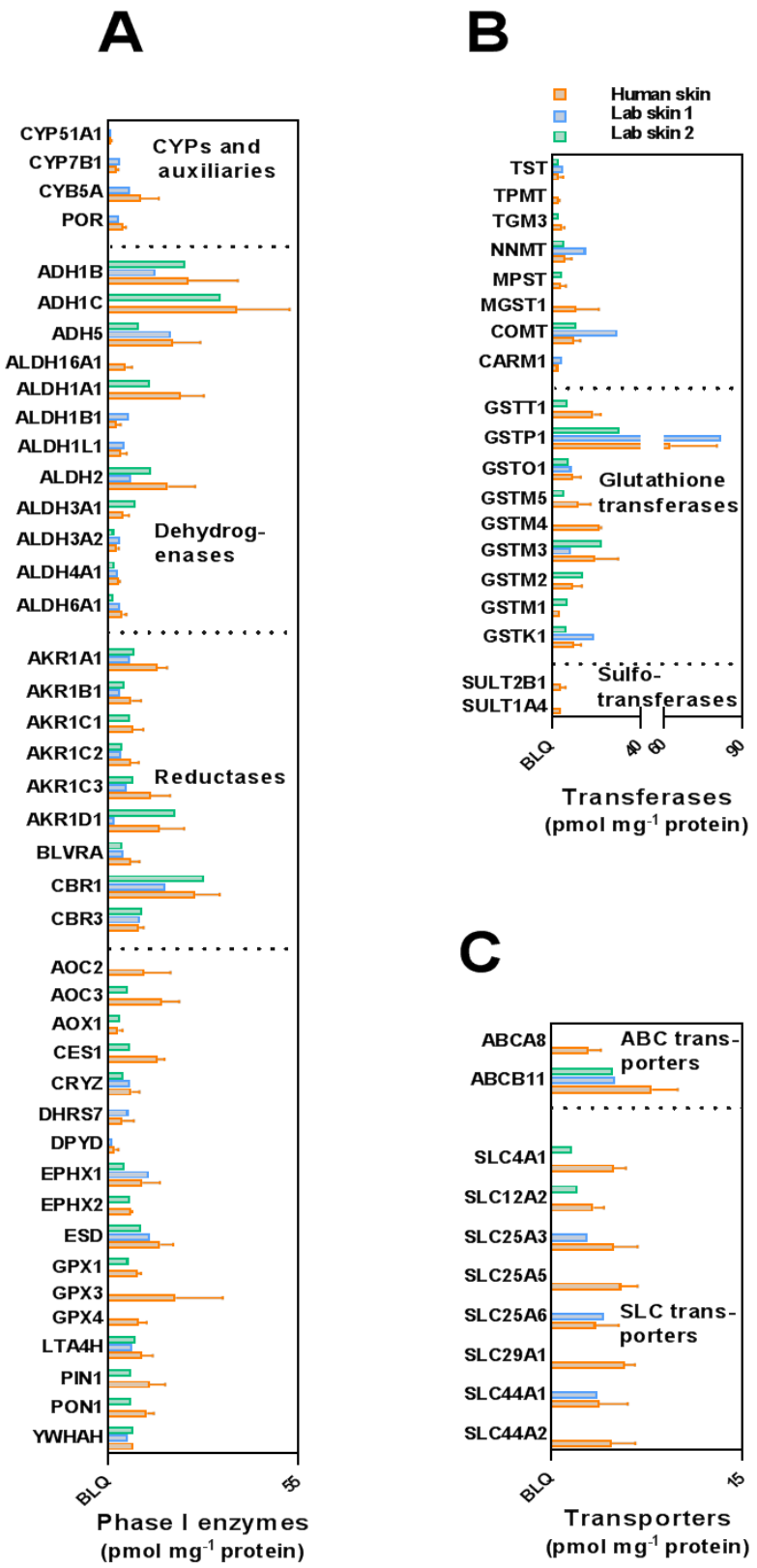
A
CYP51A1
CYP7B1
CYB5A
POR
CYPs and auxiliaries
ADH1B
ADH1C
ADH5
ALDH16A1
ALDH1A1
ALDH1B1
ALDH1L1
ALDH2
ALDH3A1
ALDH3A2
ALDH4A1
ALDH6A1
Dehydrog-enases
AKR1A1
AKR1B1
AKR1C1
AKR1C2
AKR1C3
AKR1D1
BLVRA
CBR1
CBR3
Reductases
AOC2
AOC3
AOX1
CES1
CRYZ
DHRS7
DPYD
EPHX1
EPHX2
ESD
GPX1
GPX3
GPX4
LTA4H
PIN1
PON1
YWHAH
BLQ
55
Phase I enzymes
(pmol mg-1 protein)
B
Human skin
Lab skin 1
Lab skin 2
TST
TPMT
TGM3
NNMT
MPST
MGST1
COMT
CARM1
GSTT1
GSTP1
GSTO1
GSTM5
GSTM4
GSTM3
GSTM2
GSTM1
GSTK1
Glutathione transferases
SULT2B1
SULT1A4
Sulfo-transferases
BLQ
40
60
90
Transferases
(pmol mg-1 protein)
C
ABCA8
ABCB11
ABC trans-porters
SLC4A1
SLC12A2
SLC25A3
SLC25A5
SLC25A6
SLC29A1
SLC44A1
SLC44A2
SLC trans-porters
BLQ
15
Transporters
(pmol mg-1 protein)

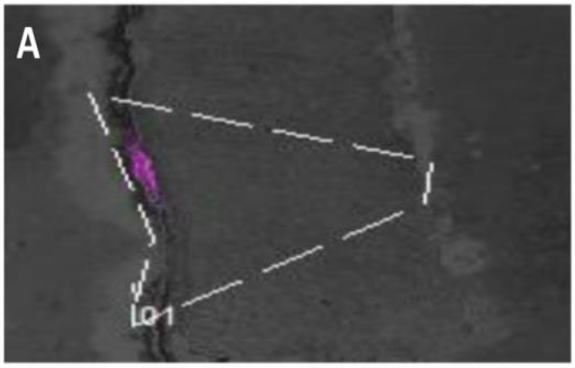
A
LO1

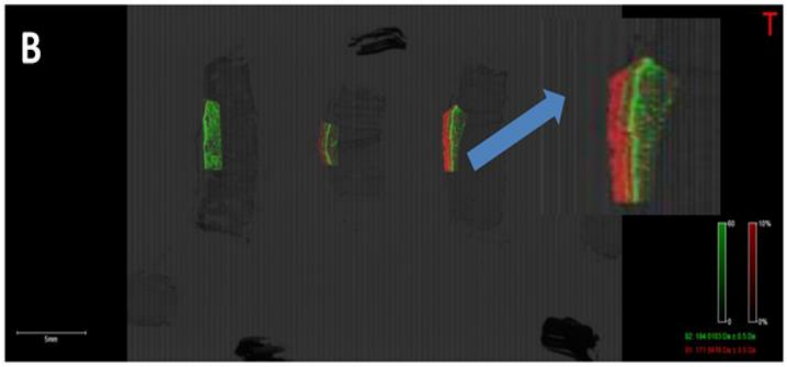
B
T

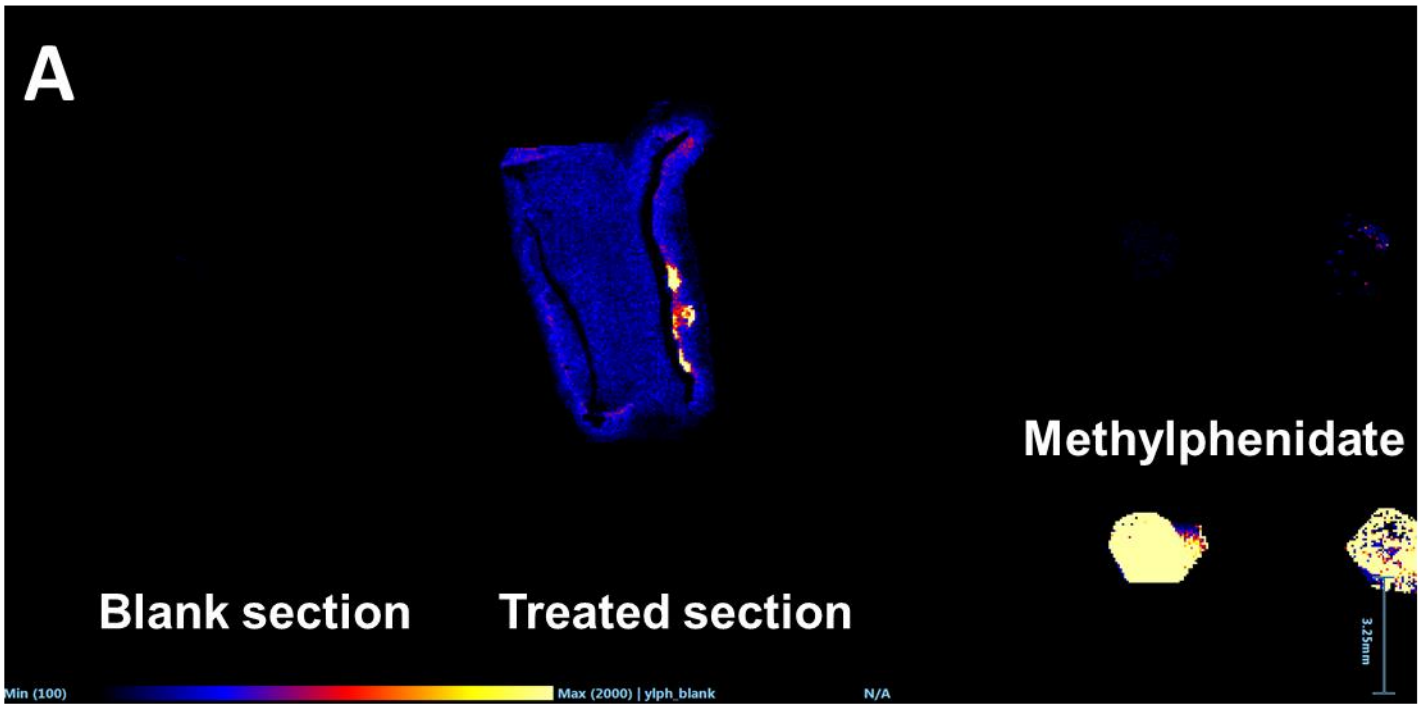
A
Methylphenidate
Blank section
Treated section
Min (100)
Max (2000) | ylph_blank
N/A
3.25mm

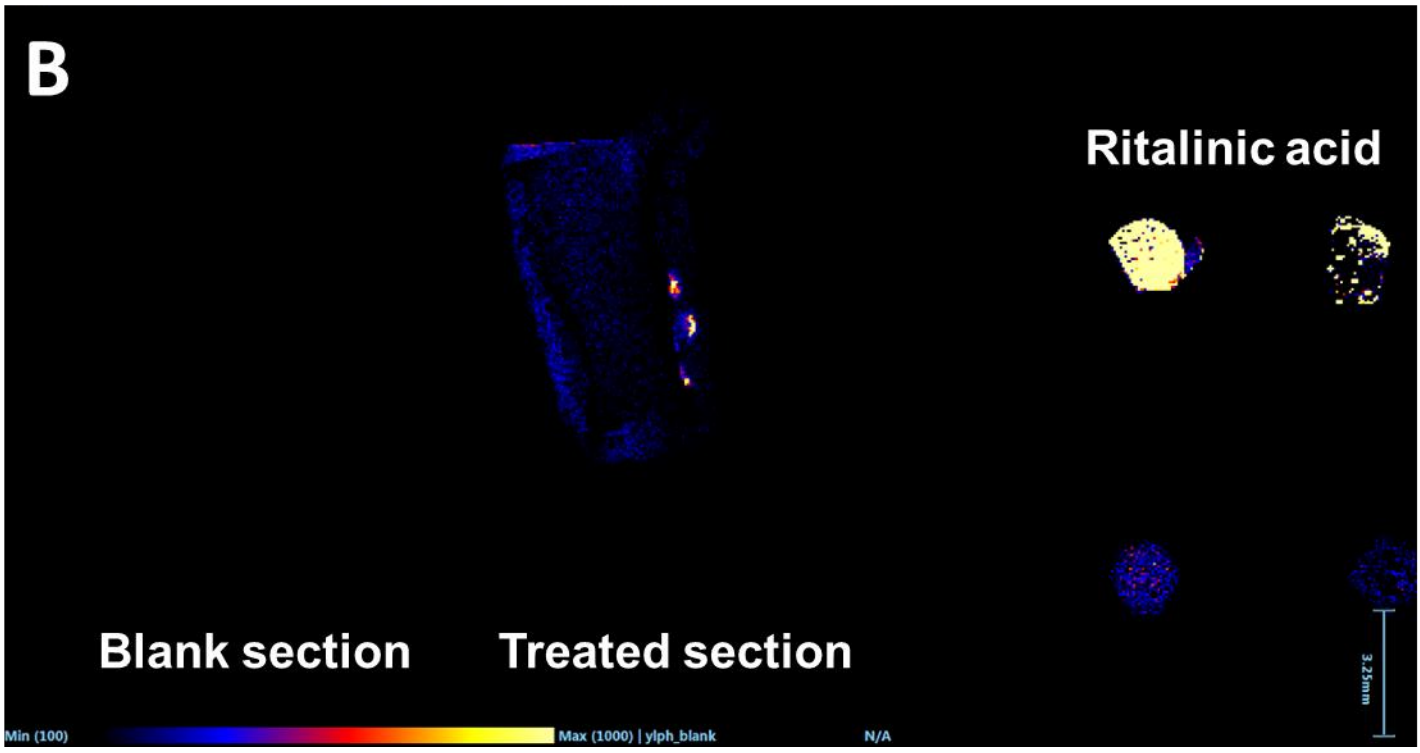
B
Ritalinic acid
Blank section
Treated section
Min (100)
Max (1000) | ylph_blank
N/A
3.25mm